BACHELOR

Laser cooling and compression of an atomic rubidium beam

Offermans, G.P.

Award date:
2015

Laser cooling and compression of an atomic rubidium beam

Bachelor End Project

Technische Universiteit Eindhoven University of Technology

Department of applied physics

G.P. Offermans - 0817698

g.p.offermans@student.tue.nl

July 2015

CQT 2015 - 07

Supervisors:

E.J.D. Vredenbregt

G. ten Haaf

Abstract

The main subject in this report is laser cooling and compression of an atomic rubidium beam. This is important to create a new kind of focused ion beam (FIB) that can keep up with the reduction in size of features in semiconductor circuits as a result of Moore's law. The goal is to get a colder atomic beam. This will result in a smaller spot size of the FIB.
First, aberrations of the telescope that deforms the cooling laser beams is investigated. These have to be minimized to obtain a colder atomic beam. Second, steering of the atomic beam is studied. This is important because the beam has to go through apertures and if the beam travels under an angle, it cannot get passed through them, so it would be useful if it can be adjusted. Third, because the steering of the beam influences on the atomic beam profile, an alternative way is researched to describe these changes. This important to understand the observed change of temperature for a steered beam.
The methods that are used are optical ray tracing as well as cooling simulations and experimental measurements. Two ways to steer the atomic beam are studied. One method involves an offset of the magnetic field and the other an imbalance of the laser intensities. The offset of the magnetic field is created by a quadrupole magnet with one coil having another current than the others. The imbalance of laser intensities is created by rotating a half-wave plate.
The results for the aberrations of the telescope are that they have a notable influence on the cooling. This is however not a significant change for the lens distance of the telescope between 10.8 cm and 11.3 cm for experimental measurements. The results of steering the atomic beam with a magnetic field is that there is a linear relation between the average transverse velocity and the offset of the magnetic field. A relation between the average transverse velocity and the intensity of one laser beam is also found for the imbalance of the laser beam intensities. For both methods the beam was not only shifted, but also acquired an angle with the longitudinal axis. While it is possible to give the atomic beam an angle with both methods, this significantly increases the temperature of the beam. This can be explained with a new description of the beam profile, which consider that if the beam gets an angle, the longitudinal velocity distribution dominates the angular distribution rather than the transverse velocity distribution. If the beam has no angle it is found that the spatial profile corresponds to a squared Lorentz function. With this new profile, it is possible to determine the temperature in an alternative way.

Contents

Chapter 1

Introduction

The semiconductor industry is an important industry today. For the research process, it is useful to ablate a part of the circuit to investigate failures and to adjust integrated circuits. One method that is in development in is to do this is with a focused ion beam.

1.1 The Focused Ion Beam

The focused ion beam (FIB) is like the scanning electron microscope (SEM). The main difference is, as the name implies, that the FIB uses ions instead of electrons. A FIB can be used for imaging, milling and deposition, see figure 1.1. The imaging process of the FIB works more or less the same as the scanning

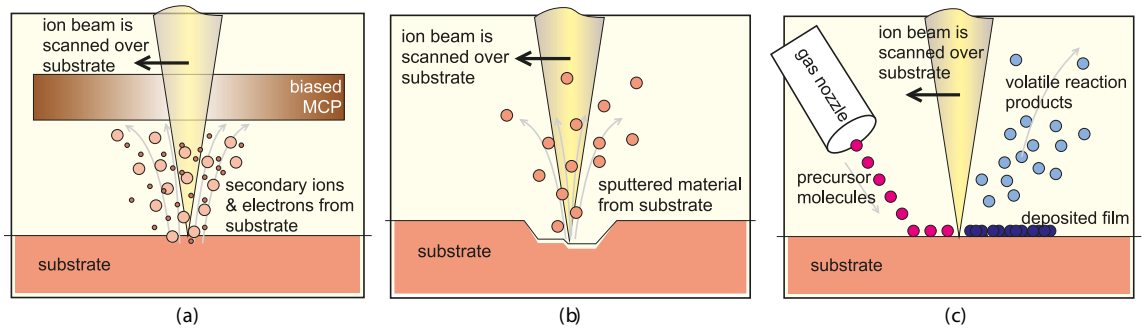

Figure 1.1: Most important applications for the FIB: (a) is imaging, (b) is milling and (c) is deposition[1].

microscope. Milling is about removing some material A gas is used together with the FIB to deposition some material.

The components in integrated circuits are reducing in size, according Moore's law. This law states that the number of transistors in an integrated circuit doubles every two years. This can also mean that the integrated circuit reduces in size. This means that the spot size of the FIB also needs to be reduced. The current generation FIB cannot keep up with Moore's law forever, so new types of FIBs have to be created. The spot size of a FIB is proportional to $\left({\sigma_U}^2/B_r\right)^{1/4}$[2], where σ_U is the energy spread of the

beam and B_r the reduced brightness. So to get a small spot size, σ_U has to be small and B_r has to be large. The brightness B is defined as

$$B = \frac{\partial^2 I}{\partial A \partial \Omega},$$

where I is the current of the beam, A its cross-sectional area and Ω the divergence. The quantity B_r is simply B/U, with U the average kinetic energy. Low temperature will result in a smaller $d\Omega$. So one possible solution to get a smaller spot size is to have an ultra-cold ion source. One potential ultra-cold ion source is the ABLIS project[3]. ABLIS stands for Atomic beam laser-cooled ion source. A schematic representation of the ABLIS is shown in figure 1.2.

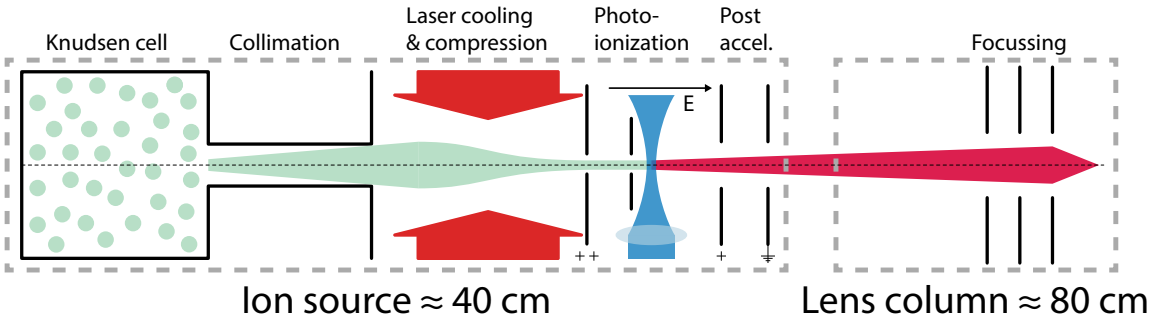

Figure 1.2: A schematic representation of the ABLIS[4]. First, an atomic beam is created with a Knudsen cell. This beam will be skimmed. After that, the atomic beam is cooled and compressed with a magnetic optical compressor. Thereafter, the atomic beam will be converted to an ion beam in the photo-ionization part. At the end the ion beam is focused.

1.2 This report

This report is my bachelor end project and is about laser cooling and compression part of the ABLIS. First the concept will be explained of laser cooling and compression in chapter 2. The theory will be covered of laser cooling/compression and how it is realized in the ABLIS. The laser beam used in the ABLIS has aberrations due cylindrical lenses. This is the first subject of this report and is discussed in chapter 3. Another problem is that the cooled laser beam has to go through an aperture. This has to be precise, so it is useful to steer the atomic beam in the cooling/compression process. This is handled chapter 4. From the results of the previous chapters, an extension of my bachelor end project is formulated and executed. This is what chapter 5 is about. The end of this report consist of a conclusion in chapter 6.

Chapter 2

Laser cooling and compression

Laser cooling is a technique to cool atoms to a temperature close to absolute zero. The cooling mechanism is based on the interaction of atoms with laser fields. In 1997, Steven Chu, Claude Cohen-Tannoudji and William D. Phillips got a Nobel Prize in Physics for this[5, 6, 7].

2.1 Theory

2.1.1 The scattering force

A laser beam can interact with an atom. This is when the frequency of the laser is around the atomic transition frequency. The result of the interaction is a force on the atom. This force is called the scattering force F_{scatt} and can be calculated with[8]

$$F_{scatt}(\delta) = \frac{\frac{1}{2}\hbar k s_0 \Gamma}{1 + s_0 + 4\delta^2/\Gamma^2}, \tag{2.1}$$

where $\hbar$ is the reduced Planck constant. The wave number of the laser is $k = 2\pi/\lambda$ (with λ the wavelength of the laser), Γ is the natural linewidth of the atom (an atomic constant). The transition rate τ is related to the the natural linewidth, with $\Gamma = 1/\tau$. Also, s_0 is the saturation parameter defined as

$$s_0 \equiv I/I_{sat}, \text{ with } I_{sat} = \frac{\pi}{3}\frac{hc}{\lambda^3}\Gamma,$$

where I is the intensity of the laser beam and I_{sat}. The detuning is defined as $\delta \equiv \omega_l - \omega_a$, with ω_l the laser frequency and ω_a the atomic resonance frequency.At first, the scattering force looks constant because all the parameters are constant. This is not the case. If the atom has no velocity v, it will get a velocity because of the scattering force. This means that the laser frequency will develop a Doppler-shift $-\underline{k} \cdot \underline{v}$. If the atom has a velocity in the same direction as the propagation direction of the laser beam, the detuning is just $\delta - kv$. The scattering force as function of the velocity is shown in figure 2.1. This force can be used to cool an atom. This technique is called Doppler cooling.

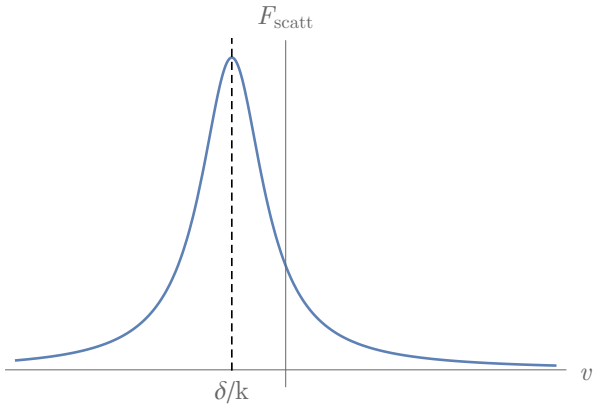

Figure 2.1: The force from equation (2.1) plotted as function of velocity. The detuning δ is negative and the maximum force is at δ/k. Typical values are a maximum force in the order of 10^{-21} N and a velocity in the order of m/s.

2.1.2 Doppler cooling

To lower the temperature T of an atom in 1 dimension, the mean square of the velocity $\langle v^2 \rangle$ has to be reduced, according to the kinetic theory. The temperature is

$$T = \frac{m \langle v^2 \rangle}{k_b}, \tag{2.2}$$

with m is the mass of the atom and k_b Boltzmann's constant. One way to achieve this is with two lasers counter propagating beams. Each laser beam, creates a force like figure 2.1 that the atom will experience. The scattering force of the two laser beams will work in opposite direction. The Doppler-shift is also the other way around. The force $F_\pm$ of one laser is then

$$F_\pm = \pm \frac{\frac{1}{2}\hbar k s_0 \Gamma}{1 + s_0 + 4(\delta \mp kv)^2/\Gamma^2}.$$

The positive force F_+ is defined as the force from the laser beam that propagate in the positive direction. The negative force F_- is from the laser beam that propagate in the negative direction. The total force F_{OM} is then

$$F_{OM} = F_+ + F_- = \frac{\frac{1}{2}\hbar k s_0 \Gamma}{1 + s_0 + 4(\delta - kv)^2/\Gamma^2} - \frac{\frac{1}{2}\hbar k s_0 \Gamma}{1 + s_0 + 4(\delta + kv)^2/\Gamma^2}. \tag{2.3}$$

A sketch is shown of equation (2.3) in figure 2.2. The figure shows that the force is equal to zero when the velocity is zero and that the force is linear in v around $v = 0$. This means that equation (2.3) can be

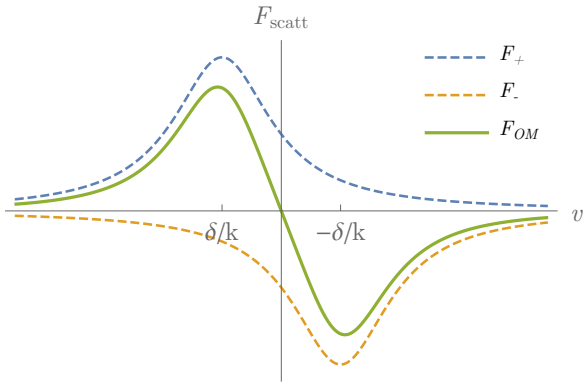

Figure 2.2: Three forces are plotted against the velocity of the atom. The positive and negative scattering force that the atom will experience are the dashed lines. The green line is the force described with equation (2.3). Around $v = 0$, the total force can be approximated with equation (2.4).

linearized around $v = 0$, so

$$\begin{aligned} F_{OM}(v) &\simeq F_{OM}(0) + v \left.\frac{\partial F_{OM}}{\partial v}\right|_{v=0} \\ &= -\beta v, \text{ with } \beta = -\frac{8k^2 s_0 \delta \hbar}{\Gamma\left(1 + s_0 + 4\delta^2/\Gamma^2\right)^2}. \end{aligned} \tag{2.4}$$

The equilibrium point of this force is at $v = 0$. For a stable equilibrium point must apply that $dF/dv < 0$. This means that $\beta > 0$ must apply. A positive β can be achieved with a negative detuning δ. In other words: an atom can only be cooled with an optical molasses (the name of this method) if the detuning is negative. An optical molasses can reach a minimum temperature T_D of

$$T_D = \frac{\hbar\Gamma}{2k_B}.$$

This is called the Doppler cooling limit[8]. The downside of an optical molasses is that the atom is cooled to $v = 0$, but not to a certain position. It is possible to cool an atom to a certain position with the help of a magnetic field. This is called the magneto optical compressor (MOC).

2.1.3 The magneto optical compressor

The Doppler-shift causes the optical molasses to cool an atom to $v = 0$. This is because the Doppler-shift is dependent on the velocity of the atom. It would be convenient that there is a frequency shift that dependent on the position of the atom. This would cause the atom to go to a certain position. This can be realized with the Zeeman effect. When the laser beams are circular polarized (opposite direction from another) and there is a magnetic field B, the Zeeman effect creates a frequency shift ω_Z. If it is a linear magnetic field with a gradient ∇B and is at $x = 0 \Rightarrow B = 0$, then the frequency shift is equal

to[8]

$$\omega_Z = \frac{g\mu_B}{\hbar}\nabla Bx, \tag{2.5}$$

where g is the Landé g-factor and μ_B the Bohr magneton. With the Doppler shift and the Zeeman effect the detuning will become $\delta_\pm = \delta \mp kv \pm \frac{g\mu_B}{\hbar}\nabla Bx$. This can be substituted in equation (2.1) and like equation (2.3), the force F_{MOC} can be calculated with

$$F_{MOC}(v,x) = \frac{\frac{1}{2}\hbar k s_0 \Gamma}{1 + s_0 + 4(\delta - kv + \frac{g\mu_B}{\hbar}\nabla Bx)^2/\Gamma^2} - \frac{\frac{1}{2}\hbar k s_0 \Gamma}{1 + s_0 + 4(\delta + kv - \frac{g\mu_B}{\hbar}\nabla Bx)^2/\Gamma^2}. \tag{2.6}$$

The Force-place plot of equation (2.6) has the same same shape as figure 2.2, only $v \to x$. This means that equation (2.6) can be approximated with a linear function in x around $x = 0$. The approximation is

$$\begin{aligned} F_{MOC}(v,x) &\simeq F_{MOC}(0,0) + v\left.\frac{\partial F_{MOC}}{\partial v}\right|_{v=0,x=0} + x\left.\frac{\partial F_{MOC}}{\partial x}\right|_{v=0,x=0} \\ &= -\beta v - \kappa x, \text{ with } \kappa = \frac{\beta g \mu_B \nabla B}{\hbar k}. \end{aligned} \tag{2.7}$$

The β is the same as equation (2.4). Equation (2.7) is the same as a damped harmonic oscillator with β as damping factor and κ as spring constant.

2.2 Simulation setup

Before experimental measurements, simulations will be used to study the effects and models. The program used to simulate the laser cooling/compression is called COOL[9]. This program can simulate one-dimensional laser cooling and compression. It can be used for different kind of atoms and situations. A screen shot is taken from this program in figure 2.3. This is an example of a simulation with

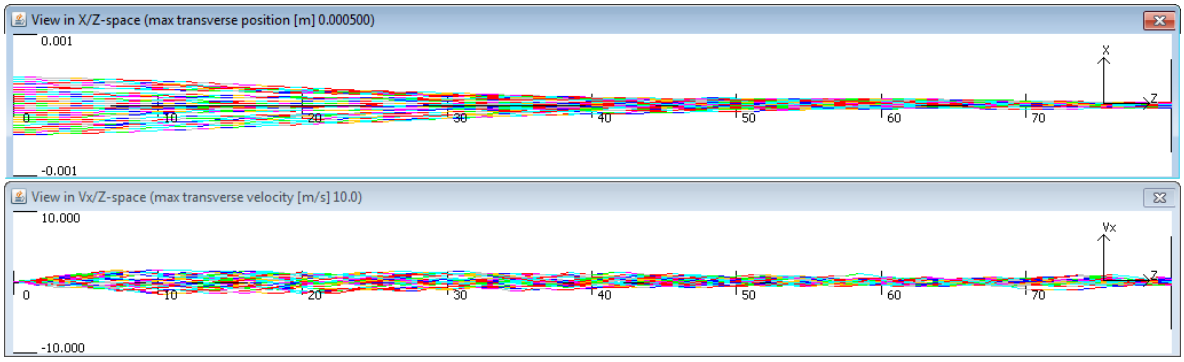

Figure 2.3: A screen shot of the simulation program COOL. The upper plot is the x/z space and the lower plot is in the v_x/z space.

cooling and compression. The compression is visible because the profile in the x/z space becomes smaller. The cooling is visible because the profile in the v_x/z space becomes smaller half way through. The x-coordinate is the transverse direction and the z-coordinate is the longitudinal direction. Important parameters for laser cooling can be modified with COOL. For example different parameter for the atomic beam source like the source type and distribution. The magnetic field gradient and offset can be modified. The saturation parameter, the beam angle and the detuning can be changed for the lasers. The output of the simulation is the velocity and place of each individual atom. These parameters are processed with Matlab.

2.3 Experimental setup

A schematic view of the experimental setup is shown in figure 2.4. The atoms used in this experiment

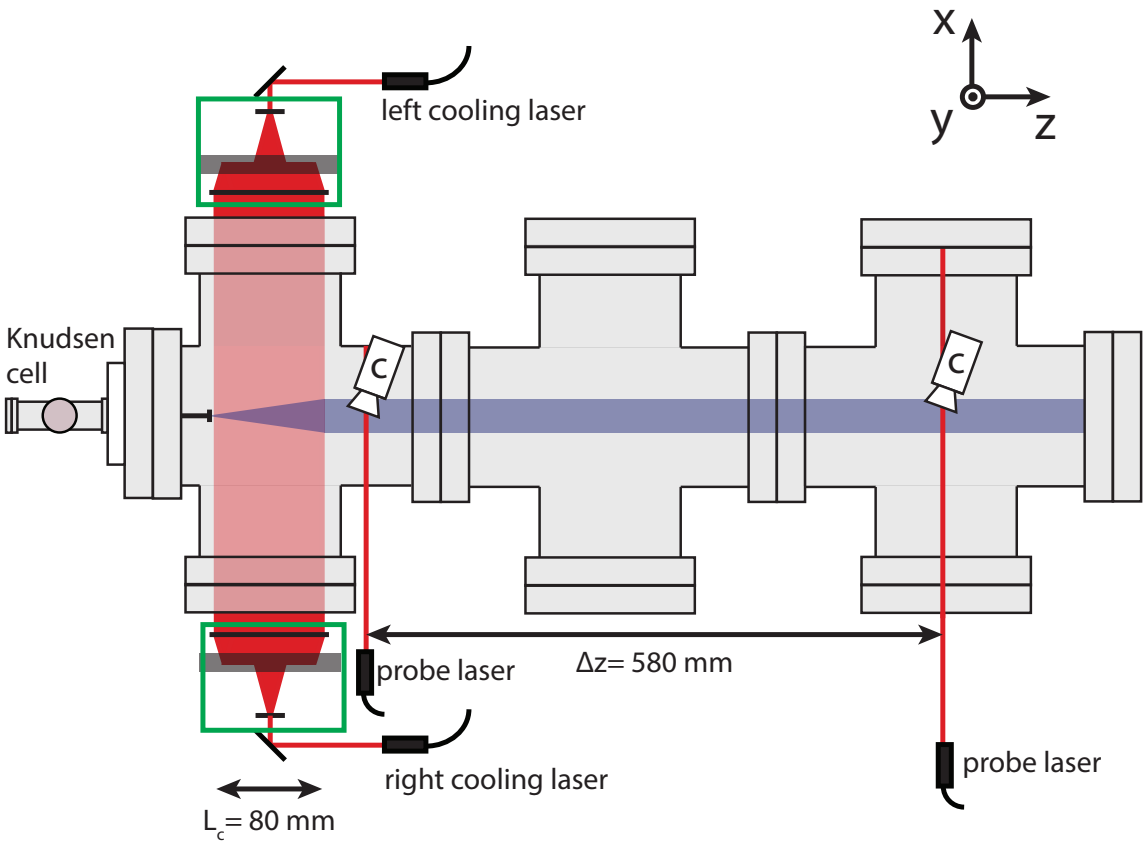

Figure 2.4: A schematic representation of the setup (top-view). Laser beams are indicated with red lines. The left and right cooling laser beam come from the same source. The intensity of the beams can be controlled independent from each other with a half-wave plate. The green boxes are the part where the telescopes are located (see section 2.3.1). The two objects that are marked with a c are the cameras to measure the beam profile. The axis are defined in the right top corner[2].

are rubidium-85 atoms. The relevant properties of Rb-85 are given in table 2.1. The source used for the atomic beam is a Knudsen cell[10]. The temperature of the source is 100 °C. The velocity of the atoms follow a Maxwell–Boltzmann distribution. This means that the average longitudinal velocity $\langle v_z \rangle \approx 305\,\text{m/s}$. The atomic beam is first collimated by a tube. This has as result that the transverse velocity distribution is approximated by a normal distribution. The two cooling laser beams come from the same laser and is with optical fibers transported to the setup. The laser power P of the two cooling lasers can be controlled independent from each other with a half-wave plate. The laser power is measured with photo diodes. The peak intensity I of a laser is related with the laser power with

$$I = \frac{P}{2\pi\sigma_y\sigma_z},$$

where $\sigma_y = 4.2\,\text{mm}$ and $\sigma_z = 34\,\text{mm}$ are the $1/e^2$-dimensions of the laser[11]. The cooling length L_c (the distance where the atom beam interact with the laser beams) is 8 mm. The cooling stage is placed in a magnetic quadrupole. This quadrupole contains four coils that can have different currents. If the currents of the coils are equal to each other, the magnetic field can be approximated with a linear field around the geometrical axis. The magnetic field gradient ∇B is proportional to the current in the coils. The maximum current is 1 A. This will result in a magnetic field gradient of $\nabla B = 7.5\,\text{T/m}$. An offset in the magnetic field can be applied, by having one coil have another current that the others. The maximum offset that can be produced is $B_0 = 1.2\,\text{mm}$. For more information about the quadrupole magnet, see the report of Van Pamelen[12].

After the cooling, a probe laser beam shines on the atom beam. This creates laser-induced fluorescence, so that the atomic beam can be seen by a camera. This camera is placed above where the fluorescence recurs. This is in the first vessel. Another laser probe beam is placed $\Delta z = 580\,\text{mm}$ after the first probe. Another camera is placed there. This is in the third vessel. The atomic beam profile can be measured with these cameras. The type of the cameras is a Grasshopper3 2.3 MP Mono USB3 Vision. The height of the camera image in the first vessel is 960 pixels and in the third vessel 600 pixels. The size of one pixel is 5.86 µm by 5.86 µm. The image is magnified with lenses. In the first vessel, the magnification factor is about 1.38 and in the third vessel about 0.19.

Figure 2.4 is just a very simplified version of the experimental setup. This is enough for our purpose because the measurements are about steering and the effects of aberrations and not about optimizing the setup. For a more detailed experimental setup, see the master´s thesis of G. ten Haaf[2] and J. van Rens[11].

2.3.1 The telescope

To increase the length of the cooling stage, the laser beam is expanded. This is done with a cylindrical telescope. The telescope consists of two lenses[1] and their properties are given in figure 2.5. The lenses are placed with flat side faced to each other at a distance d. The concave lens is the first lens of the

[1] Lenses are from Thorlabs

Table 2.1: Relevant constants of ^{85}Rb[13]

Parameter (unit)	Symbol	Value
Mass (amu)	m	84.91
Natural linewidth (MHz)	$\Gamma/2\pi$	6.07
Cooling wavelength (nm)	λ	780
Saturation intensity (W/m^2)	I_{sat}	16.7
Doppler temperature limit (μK)	T_D	146

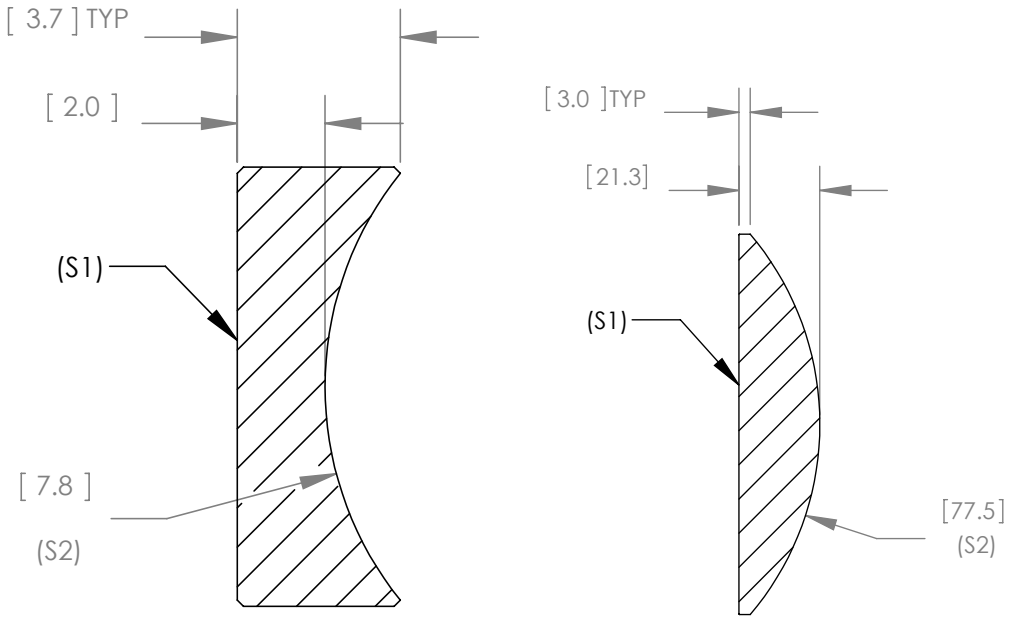

(a) LK1753L1-B($f = -15\,\mathrm{mm}$)

(b) LJ1895L1-B($f = 150\,\mathrm{mm}$)

Figure 2.5: Properties of the lenses, the unit of the measurements is in mm[14, 15].

telescope and the convex lens is the second lens. The magnification is about $|f_2/f_1| = 10$. In figure 2.6, the setup of the telescope shown. The telescope has aberrations. This is because the lenses are cylindrical. The aberrations are visible in figure 2.6 as the inequality of the distance between the rays Δy_1 and Δy_3. The aberrations of the telescope is examined in chapter 3, section 3.1.

2.3.2 Temperature and angle of the atomic beam

The two important values to measure are the angle relative to the z-axis and the temperature of the atomic beam. This will be studied in chapter 3 and 4.These values can be determined by looking at the beam profile right after the cooling, and downstream with the two cameras. The two profiles can be

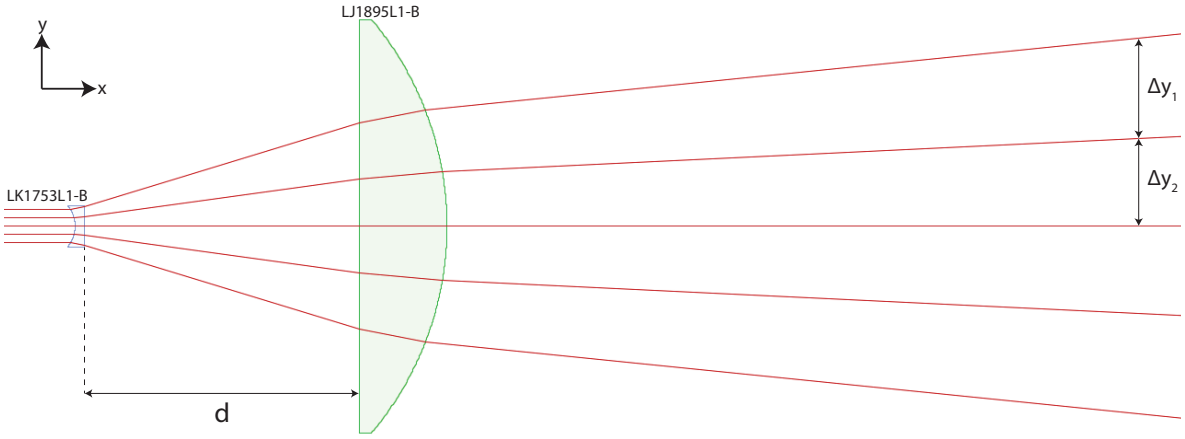

Figure 2.6: A schematic representation of the telescope with aberrations. A coordinate system is defined in the upper left corner. The red lines are light rays which are equal distributed at the left of the figure. The ray in the middle is at $y = 0$. The quantities Δy_1 and Δy_2 are the distance between two rays. The telescope has aberrations because $\Delta y_1 \neq \Delta y_2$. The lens distance in this figure is $d = 8\,\text{cm}$ (to show the aberrations).

fitted with Gaussians. The temperature T can be calculated with[11]

$$T = \frac{m}{k_B}\left(\frac{{\sigma_{x_3}}^2 - {\sigma_{x_1}}^2}{(\Delta z)^2}\right)\langle v_z\rangle^2\,, \tag{2.8}$$

where σ_{x_1} is the standard deviation of the gaussian fit in the first vessel, σ_{x_3} in the third vessel, Δz the distance between the cameras and $\langle v_z\rangle$ the average velocity of the beam in the z-direction.
If the beam makes an angle with the z-axis, it means that the beam has an average velocity in the x-direction that is not equal to zero. The average velocity is equal to

$$\langle v_x\rangle = \frac{\Delta x}{\Delta t} = \left(\frac{\langle x_3\rangle - \langle x_1\rangle}{\Delta z}\right)\langle v_z\rangle\,, \tag{2.9}$$

where $\langle x_1\rangle$ and $\langle x_3\rangle$ are the average position in the first and third vessel determined with the camera images. However, because the cameras do no align to the center of the atomic beam, the calculated transverse velocity will get an offset.
Emittance ϵ_x is a property of the atomic beam that is related to the brightness of the beam. A smaller emittance means a better atomic beam quality. This can be calculated with the other data with.

$$\epsilon_x = \sqrt{\frac{m}{2}\left(\langle x^2\rangle\langle v_x^2\rangle - \langle x v_x\rangle^2\right)}. \tag{2.10}$$

To increase the brightness, the emittance has to be reduced. The emittance is only used in the simulation part of the aberration research.

Chapter 3

The influence of aberrations on laser cooling

The telescope to magnify the laser beam consist of cylindrical lenses, see section 2.3.1. This means that there are aberrations. These aberrations can influence the cooling because it gives the beam different angles, which results in a Doppler-shift. This chapter is dedicated to check if these effects are relevant.

3.1 Aberrations of a cylindrical telescope

A sketch of the telescope is shown in figure 2.6. An x/y coordinate system is defined in this figure. To calculate analytically the angular distribution (as function of the distance between the lenses) of the telescope is complicated. It is easier to calculate it numerically. This can be done with a ray-tracing program. The ray tracing program used in this report is OpticalRayTracer[1].The lenses are symmetric in the y-axis, so the angular distribution can be approximated with an uneven polynomial as function of the y-position y of the incoming laser beam. The coefficients are dependent on the distance d between the lenses, so the angular distribution θ is approximate

$$\theta(y, d) = c_1(d)y + c_2(d)y^3 + c_3(d)y^5. \tag{3.1}$$

To get a higher brightness, this has to be reduced. This property is only studied with the simulations of the aberrations. It is now a 5th order polynomial and for a more precise approximation it can be higher order. But as it later turns out, a 5th order polynomial is enough. The angular distribution is measured with the ray tracing program for different d. The coefficients are calculated in appendix A. An example of an angular distribution is given in figure 3.1. It seems to be that equation (3.1) is a good approximation for the angle distribution and the coefficients are indeed dependent of d. The coefficients $c_n(d)$ can be

[1] http://arachnoid.com/OpticalRayTracer/

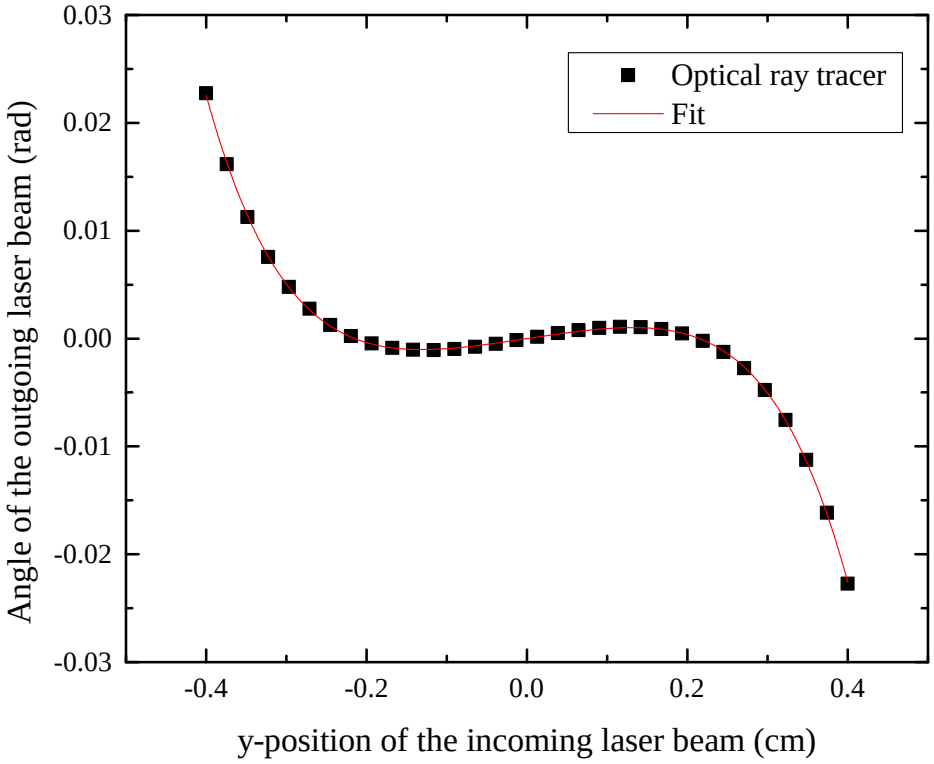

Figure 3.1: The angle of the outgoing laser beam against the y-position of the incoming laser beam measured with the ray tracing program. The fit function is equation (3.1). The distance of the lenses is $d = 12\,\text{cm}$.

approximated with a 5th degree polynomial

$$c_n(d) = \sum_{m=0}^{5} a_{n,m} d^m. \tag{3.2}$$

The values of these coefficients are calculated in appendix A and are given in table 3.1. The angular distribution can be calculated with these coefficients.

The optimal lens distance is defined as the distance with the smallest average absolute angle $\overline{\theta}$. The average angle can be calculated with

$$\overline{\theta} = \frac{1}{2r} \int_{-r}^{r} |\theta(y, d)| \, dy,$$

Table 3.1: An overview of the coefficients from equation (3.2) for the telescope. The unit of these coefficients are cm^{1-2n-m}

m \ n	1	2	3
0	0.54737	0.30299	0.46139
1	-0.06190	-0.02101	-0.10438
2	0.00574	-0.00259	0.02796
3	$-8.54824 \cdot 10^{-4}$	$5.65069 \cdot 10^{-4}$	-0.00611
4	$5.93854 \cdot 10^{-5}$	$-7.69273 \cdot 10^{-5}$	$5.87672 \cdot 10^{-4}$
5	$-1.56438 \cdot 10^{-6}$	$3.02715 \cdot 10^{-6}$	$-2.70534 \cdot 10^{-5}$

where r is the maximum y-position. The cooling length is $L_c = 8\,\text{cm}$ and the magnification of the telescope is approximately $f_2/f_1 = 10$, so $r \approx 4\,\text{mm}$. The average angle against the lens distance is calculated numerically and shown in figure 3.2. According to this figure, the optimal distance is

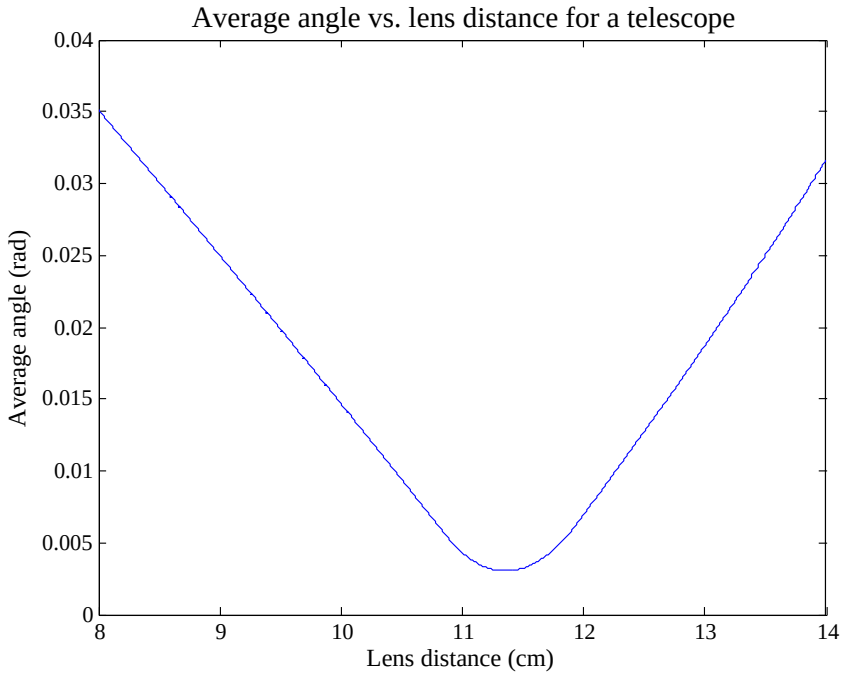

Figure 3.2: The Average angle $\overline{\theta}$ against the lens distance d. The minimum $\overline{\theta}$ is at $d = 11.36\,\text{cm}$.

at $d = 11.36\,\text{cm}$. At that distance, the laser cooling is expected to be at his best. The effects of the aberrations are probably when the Doppler-shift ω_D is approximately the natural linewidth. This is because then the force of equation (2.3) is at his maximum. The assumption is made that the atom has no transverse velocity, so $\omega_D = kv_z \sin\theta \simeq \Gamma$. With the parameters of table 2.1 and the mean longitudinal velocity is $\langle v_z \rangle \approx 305\,\text{m/s}$ the angle where the aberrations will play a part is $\theta \simeq 0.023$.

Table 3.2: Parameters used in the simulations. The top part of the list is about the source, the middle part about the intervals in general and the bottom about the laser. The atoms used are Rb-85, see table 2.1.

Parameter (unit)	Value
Maximum position (mm)	1
Maximum velocity (m/s)	0
Average speed (m/s)	200
Spread in speed (m/s)	0
Length (mm)	0.625
On-axis magnetic field (G)	0
x-gradient magnetic field (T/m)	2
Saturation parameter (-)	1
Detuning (linewidths)	-0.5

3.2 Simulations

Simulations are used to study the effect of aberrations on the laser cooling. To apply the angular distribution to the simulation, the simulation contains 80 equally large intervals with each a different laser angle according to the angle distribution. The conditions for the simulations are given in table 3.2.

The first simulations are with 500 atoms. The results of the first simulations are shown in figure 3.3. The temperature is calculated with equation (2.2) and the emittance with equation (2.10). The cooling is the most effective around $d = 11.5$. To find the optimal lens distance, simulations are done around $d = 11.5$ with 50000 atoms for more accuracy. The results are shown in figure 3.4. These results say that the optimal lens distance is between 11.3 and 11.7 and this corresponds to the lens distance with the minimal $\overline{\theta}$.

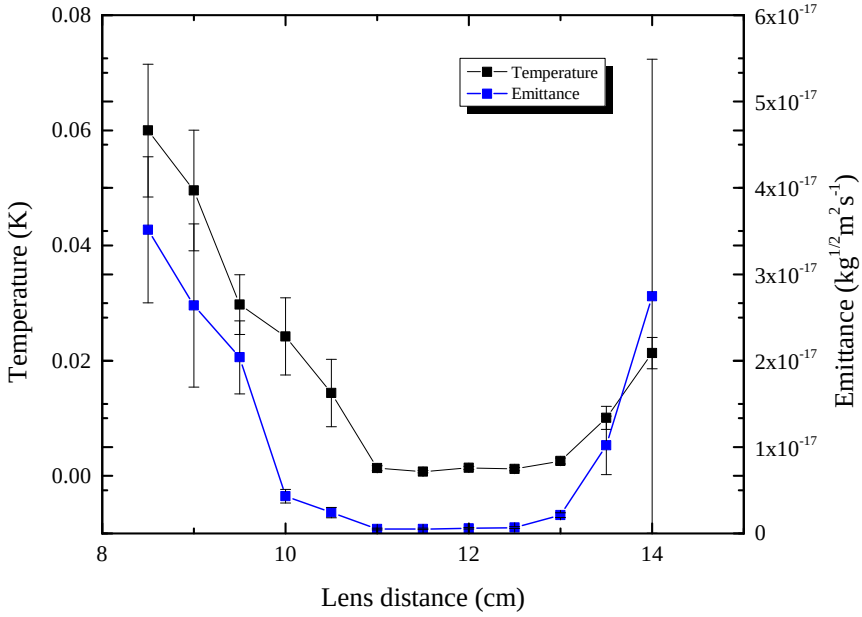

Figure 3.3: Results of the simulations with 500 atoms. The temperature and emattance are plotted against the lens distance.

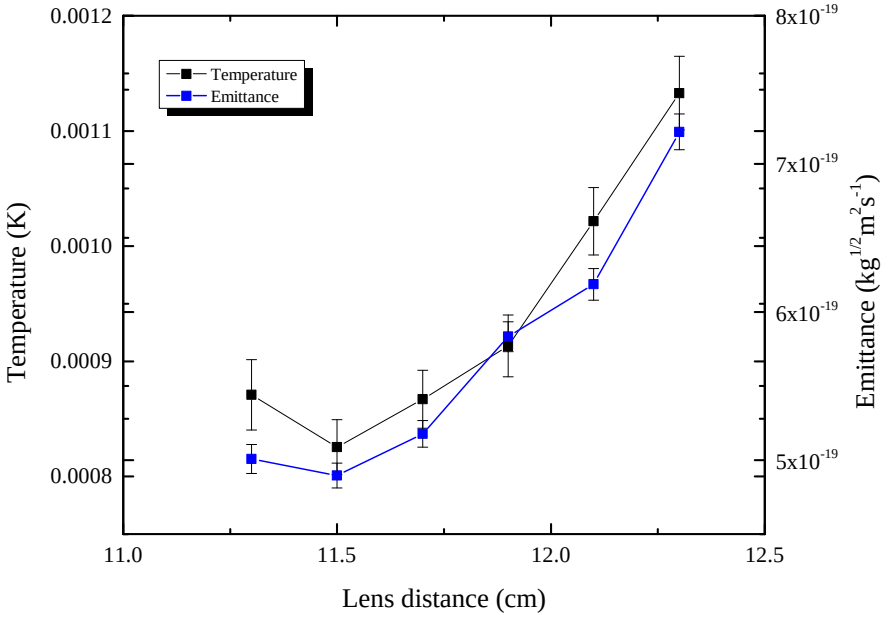

Figure 3.4: Results of the simulations with 50000 atoms. The temperature and emattance are plotted against the lens distance.

3.3 Experiments

The ABLIS telescope has normally a lens distance of 11.02 cm. To verify if this is the optimal distance for cooling, a scan is done to measure the temperature of the beam for different lens distances. The profiles are shown in figure 3.5. The temperature is calculated with equation (2.8) and is plotted in figure 3.6 as

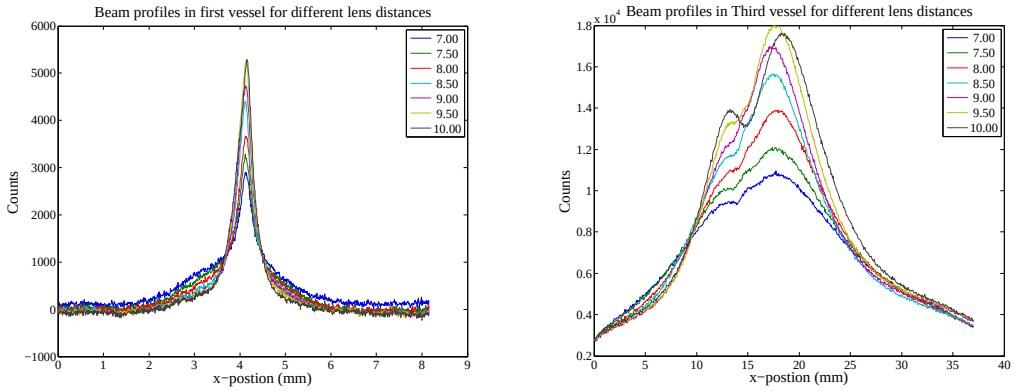

(a) Profile in the first vessel

(b) Profile in the third vessel

Figure 3.5: The beam profiles for different lens distances. The values in the legend are the lens distances with unit cm. It is cooling and compression with no imbalance in laser intensity and no offset in the magnetic field. important parameters are $\nabla B = 0.75\,\mathrm{N/m}$ and $\delta = -3.8\,\mathrm{MHz}$.

function of the lens distance. According to the temperature plot, the optimal lens distance is between

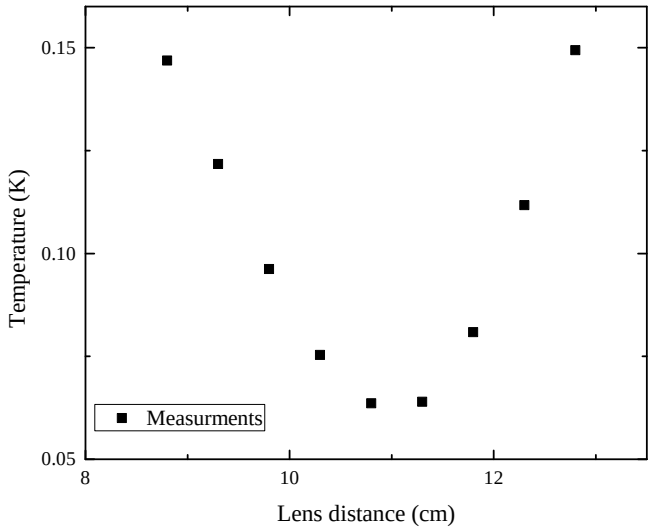

Figure 3.6: The temperature of the atomic beam as function of the lens distance.

10.8 cm and 11.3 cm. This is just under the predicted lens distance. But it is very close and the 0.5 cm

has little effect according the graph.

3.4 Conclusion

The prediction for the beam angle that has an effect on the cooling is $\theta \approx 0.023$. The predicted optimal lens distance is $d = 11.36\,\text{cm}$. According to the simulations the optimal lens distance is between 11.3 cm and 11.5 cm. The optimal lens distance is according the experiments between 10.8 cm and 11.3 cm. Around these ranges the aberrations have not much influence on the temperature of the cooled atomic beam. The predicted optimal lens distance does agree with the simulations but not with the experiments. It is however not a major difference.

Chapter 4

Steering a laser-cooled atomic beam

After the cooling and compression stage of the ABLIS, the atomic beam has to go through two apertures before reaching the photo-ionization process, see figure 1.2. It is possible that the atomic beam the cooling stage leaves with an angle with the z-axis. It is also possible that the beam has not the same transverse position as the two apertures. In both cases, the beam can hit the side of the aperture, so that the beam does not continue to the photo-ionization process. This should not happen. It would be convenient to steer the atomic beam in the cooling and compression process. This would mean that the atomic beam can be corrected so, that it goes through the apertures. In this chapter, two methods are discussed to steer the atomic beam. The first method is to apply an offset to the magnetic field of the compressor. The second method is with an imbalance between the intensities of the two cooling laser beams.

4.1 An offset in the magnetic field

When an offset B_0 is applied to the magnetic field, it has an effect on the Zeeman-shift. The magnetic field can be written as $B^* = \nabla B\, x + B_0$ and the Zeeman frequency (equation (2.5)) is then $\omega_Z = \frac{g\mu_B}{\hbar}(\nabla B\, x + B_0)$. This shift can be substituted as in equation (2.6) and it can be linearized as in equation (2.7). This gives

$$F_{MOC} = -\beta v_x - \kappa\left(x + \frac{B_0}{\nabla B}\right). \tag{4.1}$$

Because the force is dependent on x and v_x, the system can only be in balance ($F_{MOT} = 0$) for $v = 0$ and $x = x_0$. For equation (4.1) $x_0 = -\frac{B_0}{\nabla B}$. This means it is a damped oscillator with an offset. If the cooling length is infinite, the beam will have $\langle x\rangle = x_0$ and $\langle v_x\rangle = 0$ at the end. This means that the beam is shifted and has no angle angle with th z-axis. But if the cooling length is small, the oscillator is still damping to the offset, which will result in $\langle v_x\rangle \neq 0$. Equation (4.1) is a differential equation with $x(0) = u$ (u is a constant) and $v_x(0) = x'(0) = 0$, because we assume that $\langle v_x\rangle = 0$, at $t = 0$. The

solution of this differential equation is

$$x(t) = \frac{1}{2\alpha} e^{-\frac{t(\beta+\alpha)}{2m}} \left(u \left(\beta \left(e^{\frac{\alpha t}{m}} - 1 \right) + \alpha \left(e^{\frac{\alpha t}{m}} + 1 \right) \right) - x_0 \left(\alpha \left(-2e^{\frac{t(\alpha+\beta)}{2m}} + e^{\frac{\alpha t}{m}} + 1 \right) + \beta \left(e^{\frac{\alpha t}{m}} - 1 \right) \alpha \right) \right), \tag{4.2}$$

with $\alpha = \sqrt{\beta^2 - 4m\kappa}$. The velocity v_x is the time derivative of equation (4.2) and is

$$v_x(t) = \frac{1}{4m\alpha}(\alpha - \beta)(\alpha + \beta)\,(u - x_0) \left(e^{\frac{\alpha t}{m}} - 1 \right) e^{-\frac{t(\alpha+\beta)}{2m}}. \tag{4.3}$$

To get the average of v_x, equation (4.3) has to be integrated over u from -r to r (r is the radius of the source) and that has to be divided by the range length, so $2r$. The velocity at the end of the laser cooling has to be calculated. This is at $t = L_c / \langle v_z \rangle$. So

$$\begin{aligned} \langle v_x \rangle &= \frac{1}{2r} \int_{-r}^{r} v_x(L_c / \langle v_z \rangle)\, du \\ &= -\frac{x_0}{4m\alpha}(\alpha - \beta)(\alpha + \beta) \left(e^{\frac{\alpha L_c}{m\langle v_z \rangle}} - 1 \right) e^{-\frac{(\alpha+\beta)L_c}{2m\langle v_z \rangle}}. \end{aligned} \tag{4.4}$$

To get a feeling for the value of the average transverse velocity, values of tables 2.1 and 4.1 are filled in equation (4.4). If the Magnetic field offset is just 0.0002 Tesla, the average transverse velocity is -0.5 m/s. All the parameters in equation (4.4) are independent of x_0. This means that

$$\langle v_x \rangle \propto x_0. \tag{4.5}$$

Because $x_0 = -\frac{B_0}{\nabla B}$, it is expected that there is a linear relation between the B_0 and $\langle v_x \rangle$ (the angle of the beam). This calculation can also be done for $\langle x \rangle$. The results that $\langle x \rangle$ is also proportional to x_0, so a linear relation with B_0. The offset in the magnet field creates a displacement of the atomic beam, but because the cooling length is finite, the atomic beam also gets an angle $\langle v_x \rangle$ / $\langle v_z \rangle$.

4.2 An imbalance in the intensity of the laser beams

Steering is also possible with an imbalance in laser intensity. However, this is a bit more complicated than a shift with an offset in the magnetic field. To simplify things, laser cooling without compression is studied. With an imbalance in laser intensity (the + laser has saturation s_1 and the - laser s_2), equation (2.3) has to be rewritten to

$$F_{OM} = \frac{\frac{1}{2}\hbar k s_1 \Gamma}{1 + s_1 + 4(\delta - kv)^2/\Gamma^2} - \frac{\frac{1}{2}\hbar k s_2 \Gamma}{1 + s_2 + 4(\delta + kv)^2/\Gamma^2}. \tag{4.6}$$

The linear approximation of equation (4.6) will be

$$F_{OM} \simeq -\beta(v - v_0), \text{ with } \beta = -\frac{4k^2\delta\hbar}{\Gamma}\left(\frac{s_1}{(1+s_1+4\delta^2/\Gamma^2)^2} + \frac{s_2}{(1+s_2+4\delta^2/\Gamma^2)^2}\right)$$
$$\text{and } v_0 = \frac{1}{2}k\Gamma\left(\frac{s_1}{1+s_1+4\delta^2/\Gamma^2} - \frac{s_2}{1+s_2+4\delta^2/\Gamma^2}\right)/\beta. \tag{4.7}$$

With the boundary condition $v(0) = 0$ (because $\langle v_x \rangle = 0$ at $t = 0$), the solution of the differential equation of equation (4.7) is

$$v(t) = v_0\left(1 - e^{-\beta t/m}\right).$$

The average mean velocity is then $\langle v_x \rangle = v(L_c/\langle v_z \rangle)$. For the values given in tables 2.1 and 4.2 but with an imbalance of $s_1 = 1.5$ and $s_2 = 2.3$ the factor $\beta = 3 \cdot 10^{-21}$ kg s^{-1}. The value of the exponential part will is then $e^{-\beta L_c/\langle v_z \rangle m} = 0.04$. The transverse velocity will be then 0.5 m/s. Now is β dependent of s_1 and s_2. This means that $\langle v_x \rangle$ is not proportional to v_0, expect when there is an infinite cooling length, but that is not the case. So the average velocity is

$$\langle v_x \rangle = \frac{\Gamma^2}{8k\delta}\frac{s_1 s_2(\alpha_1 - \alpha_2)}{{\alpha_1}^2 s_2 + {\alpha_2}^2 s_1}\left[\exp\left(\frac{4k^2\delta\hbar L_c}{m\Gamma v_z}\left(\frac{{\alpha_1}^2}{s_1} + \frac{{\alpha_2}^2}{s_2}\right)\right) - 1\right], \tag{4.8}$$

with

$$\alpha_n = \frac{s_n}{1 + s_n + 4\delta^2/\Gamma^2}.$$

4.3 Simulations

To verify if equations (4.4) and (4.8) are good approximations, simulations are done.

4.3.1 Offset in the magnetic field

Simulations can be used to verify the linear relation between the B_0 and $\langle v_x \rangle$. The parameters used in the simulations are given in table 4.1. Further information about the simulation is that the source has a uniform transverse an longitudinal velocity distribution and aberrations of the laser beams are not included. The offset B_0 is the variable of the simulations and has a range from -3 to 3 G and the measured value is the average velocity at the end of the simulation. The results of the simulations are given in figure 4.1. The results of the simulations have a slightly lower slope than the analytical model. It seems like that the analytical model describes the average transverse velocity of the simulations. The results show that there is indeed a linear relation between the offset of the magnetic field and the angle of the beam. If $|B_0| > 3$, the relation is becoming less linear. This is because the offset has shifted the force away from the point where the force can be approximated with (2.7). The analytical model, equation (4.4), is also plotted in figure 4.1.

Table 4.1: Parameters used in the simulations for the offset in magnetic field. The top part of the list is about the source, the middle part about the interval and the bottom about the laser. The atoms used are Rb-85, see 2.1. These parameters are based on a article of Wouters *et al*[16].

Parameter (unit)	**Symbol**	**Value**
Number of atoms (-)		400
Maximum position (mm)	r	0.21
Maximum transverse velocity (m/s)	v_x	0
Average longitudinal velocity (m/s)	$\langle v_z \rangle$	309
Spread in speed longitudinal velocity (m/s)	σ_{v_z}	0
Length (m)	L_c	0.05
x-gradient magnetic field (T/m)	∇B	1
Saturation parameter (-)	s_0	0.67
Detuning (linewidths)	δ	-0.5

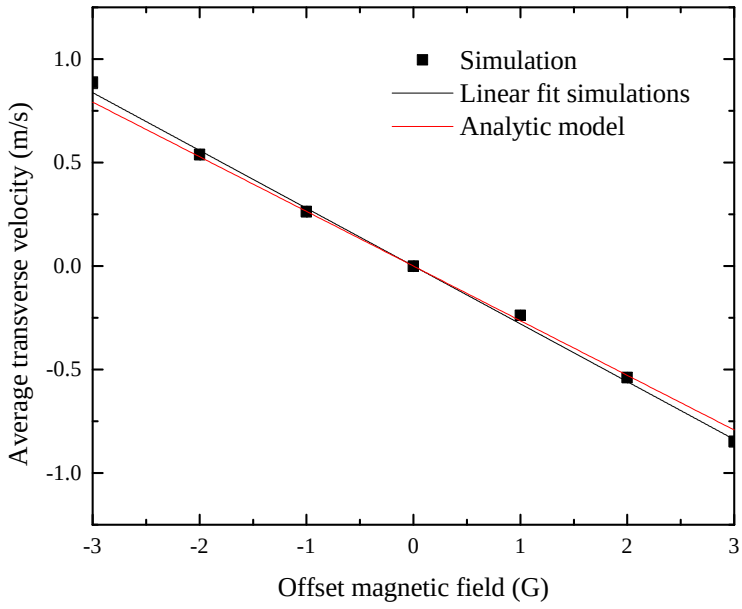

Figure 4.1: The average transverse velocity of the atomic beam against the offset of the magnetic field offset. The results of the simulations and the analytical model (equation (4.8)) are shown for the parameters of tables 2.1 and 4.1.

4.3.2 Imbalance in the laser intensities

The parameters used for the simulations with the imbalance are given in table 4.2. The variable parameter for these simulations is s_2 (the left cooling laser). The results are shown in figure 4.2.
According the figure it is possible to give an atomic beam an average transverse velocity. In other words, an atomic beam can get an angle with the z-axis if there is an imbalance between the laser beam inten-

Table 4.2: Parameters used in the simulations for the imbalance of laser beam intensities. The top part of the list is about the source, the middle part about the interval and the bottom about the laser. The atoms used are Rb-85, see 2.1.

Parameter (unit)	**Symbol**	**Value**
Number of atoms (-)		200
Maximum position (mm)	r	1
Maximum transverse velocity (m/s)	v_x	0
Average longitudinal velocity (m/s)	$\langle v_z \rangle$	305
Spread in speed longitudinal velocity (m/s)	σ_{v_z}	0
Length (m)	L_c	0.08
x-gradient magnetic field (T/m)	∇B	0
Saturation parameter right cooling laser (-)	s_1	2.3
Detuning (linewidths)	δ	-0.5

sities. The relation between the average transverse and the saturation parameter of the left laser looks a bit linear according the simulations, only with a small curve. This agrees with the analytical model, equation (4.8). This simulations agree with the model according to the figure. Therefore The analytical model is correct for the simulations.

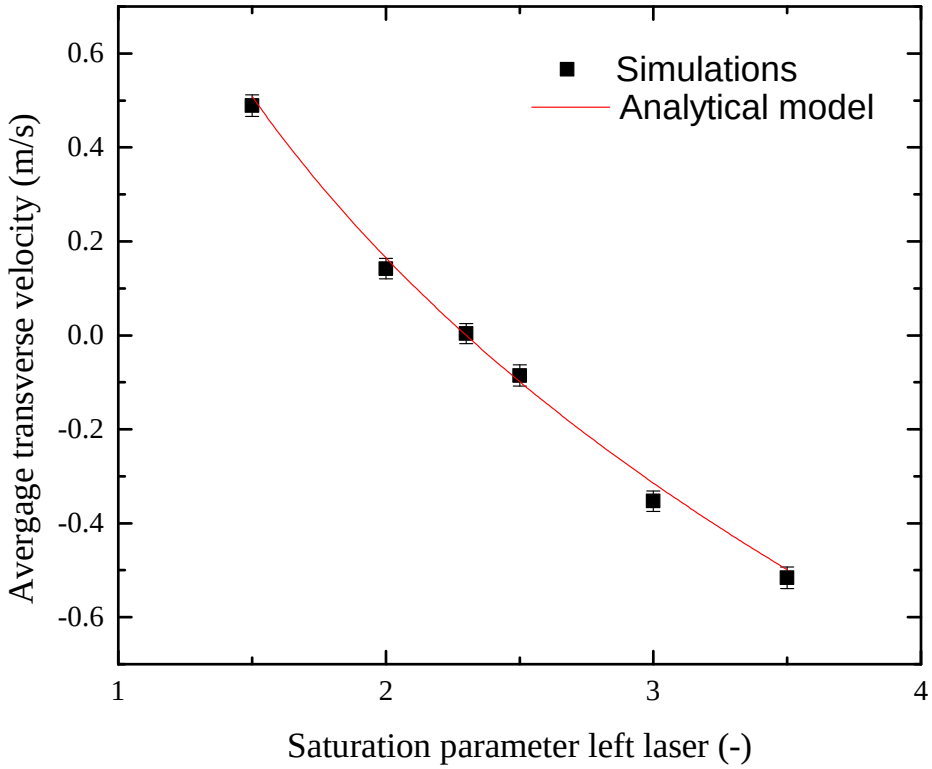

Figure 4.2: The average transverse velocity of the atomic beam against the saturation parameter of the left laser (s_2). The results of the simulations and the analytical model (equation (4.8)) are shown for the parameters of tables 2.1 and 4.2.

4.4 Experiments

In the previous section steering of an atomic beam is studied with simulations. This section is dedicated to experimental results. The coordinates are defined in figure 2.4. A positive transverse position (x-position) is down and a negative transverse position is up in the figure. The setup is viewed in this section in the propagating direction of the atomic beam. So left is in the transverse direction positive and right in the transverse direction negative.

4.4.1 Offset in the magnetic field

To create an offset in the magnetic field, one coil of the quadrupole magnet should have a different current than the other coils. The displacement of the magnetic field is proportional to the current of the variable coil. For these experiments the other coils had a current 0.01 A. If the variable coil has also this current, the magnetic field gradient would be around 0.3 T/m. For a more detailed explanation

about the gradient and the offset of the magnetic field, see the report of Van Pamelen[12]. The detuning is here $\delta = 3.8\,\text{MHz}$ and the two cooling lasers have $s_0 = 2.2$.
For this experiment, the variable coil is the right coil and the current is scanned from 0 to 0.1 A. In figure 4.3 the beam profile is shown for different currents. It is in the figure that for increasing current,

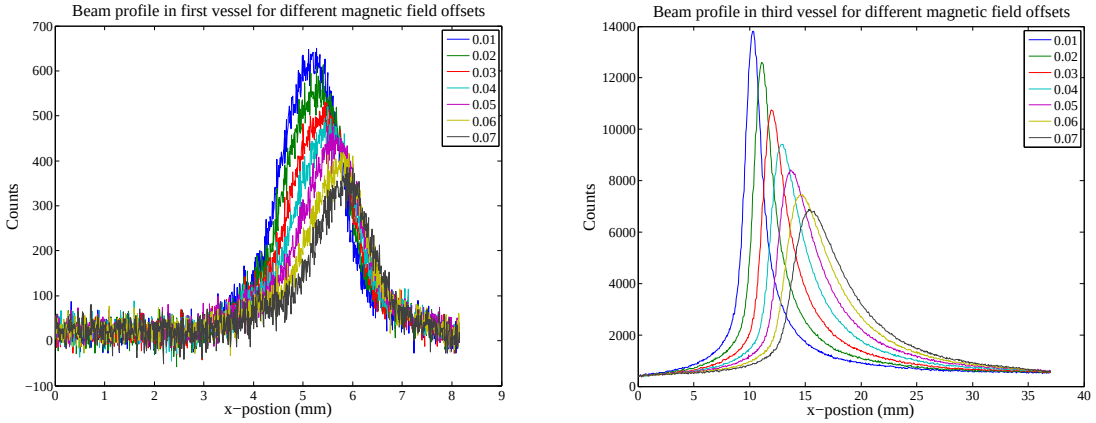

(a) Profile of the first vessel

(b) Profile of the third vessel

Figure 4.3: The beam profiles for different currents of the right coil. Values of the legend are the current in Ampere.

the profiles shift to the left (to the right in the figures). This is clearly visible for both vessels. This is expected because the offset in the magnetic field creates an offset in the damped harmonic oscillator.
With these profiles the transverse velocity and the temperature are calculated with equations (2.9) and (2.8). The transverse velocity is plotted in figure 4.4. According these results, the relation between the average transverse velocity and the current of the right coil is linear. The current of the right coil has a linear relation for the offset in the magnetic field for this range, so the linear relation between the offset of the magnetic field and the average traverse velocity is as predicted according equation (4.5). A quantitative comparison between the results and equation (4.4) is not made. This is because the quantitative relation of the magnetic field offset and the current is not measured for these circumstances. When the right coil has a current of 0.01 A (the same as the rest). The velocity is not equal to zero as expected. This is because the two cameras are not placed exactly in the middle of the beam. This is the reason for the offset in the figure.
The temperature is plotted against the current of the right coil in figure 4.5. The temperature is the lowest around the point that the coils have the same current. A bigger offset means a higher temperature. There is no model made to predict the temperature of the atomic beam when there is an offset in the magnetic field. From the results a conclusion can be made that it is possible to give the cooled atomic beam an angle with the z-axis. It was as predicted a linear relation. However, when the atomic beam is steered to hard, the temperature will increase significantly.

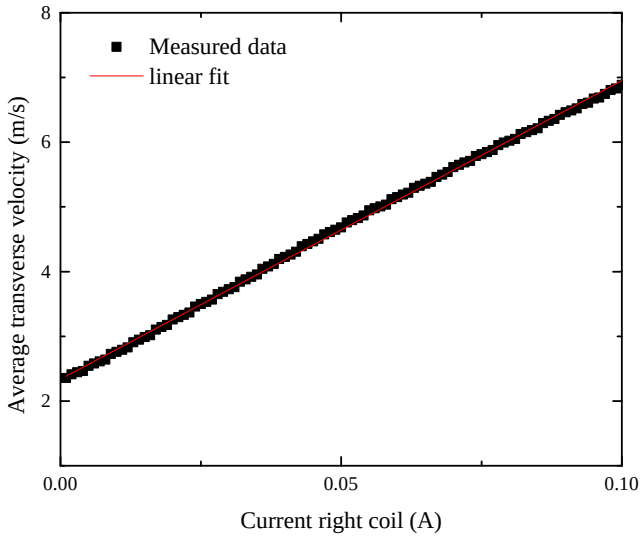

Figure 4.4: The measured average transverse velocity against the current of the right coil. A linear fit is made for the experimental data.

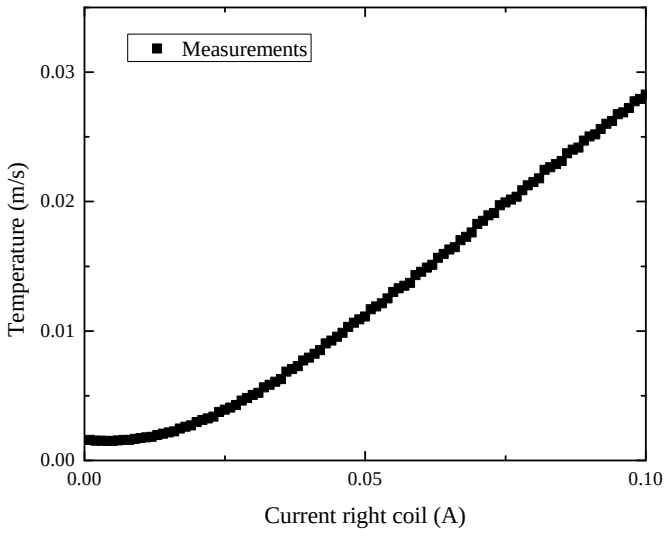

Figure 4.5: The measured temperature of the atomic beam against the current of the right coil.

4.4.2 Imbalance in the laser intensity

The intensity of the laser beams can be adjusted by rotating a half wave plate. The intensity of the right laser beam is held constant. The saturation parameter for this beam is $s_{right} = 2.3$. The detuning of the two lasers is $\delta = 3.8\,\text{MHz}$. There is also no magnetic field. The measured profiles are shown figure 4.6. In the first vessel and third vessel, the beam profile shifts to the left (to the right in the

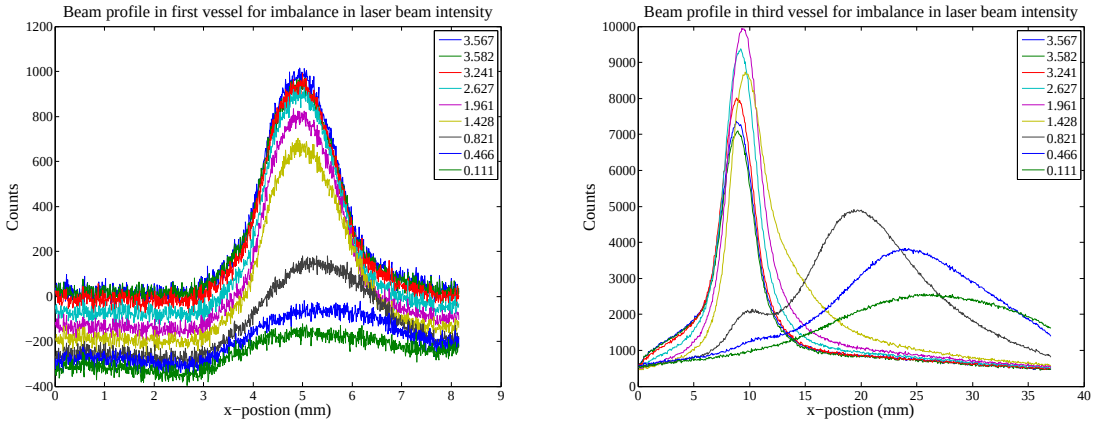

(a) Profile of the first vessel

(b) Profile of the third vessel

Figure 4.6: The beam profiles for different laser beam intensities of the left laser beam. Values of the legend are the saturation parameter of the left laser beam.

graphs) for decreasing left saturation parameter. This this shift in profiles is because the beam has an angle with the z-axis. The shift is not really visible in the first vessel and in the third vessel only for low saturation parameters. Another strange phenomenon is that in the third vessel for small saturations, a small peak occurs. This is currently unexplained why. Like the previous measurements, the transverse velocity and the temperature is determined. The measured profiles with two peaks are removed from this calculations, because the position and standard deviation cannot be determined with one Gaussian. The results of the transverse velocity for the different intensity is shown in figure 4.7. This is done for the experimental data and the analytical model, equation (4.8). Both are linear relations with a small curve, like the simulations. When the saturation parameter of the left laser beam is increased, the average transverse velocity decreases. The analytical model and the experimental data have the same shape but do not overlap. This has been the case by the simulations. One reason could be that the approximation is made that the transverse velocity is zero at the beginning of the cooling. This assumption is made because the average transverse velocity is zero. This distribution was the case with the simulations. However, the transverse velocity distribution can be approximated with a Gaussian distribution. This can be the missing part of the model.

The temperature is also calculated of the atomic beam and is plotted in figure 4.8. The temperature is at his lowest point when the two laser beams intensities are approximately in balance. The temperature increases when the angle with the z-axis increases. This is the same with the magnetic field offset.

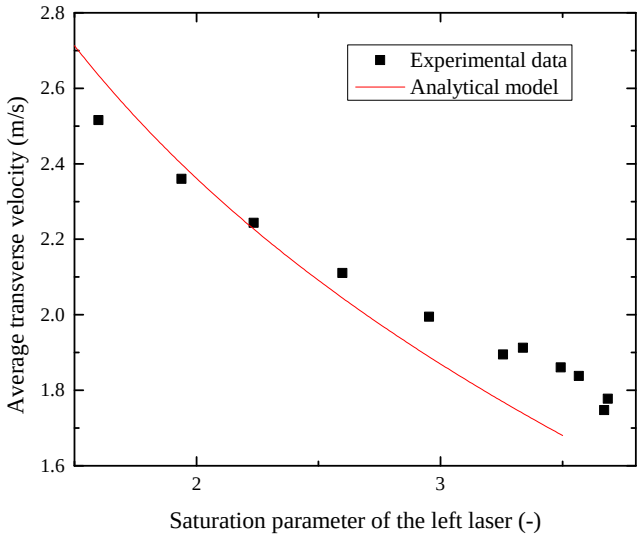

Figure 4.7: The average transverse velocity against the saturation parameter of the left laser.

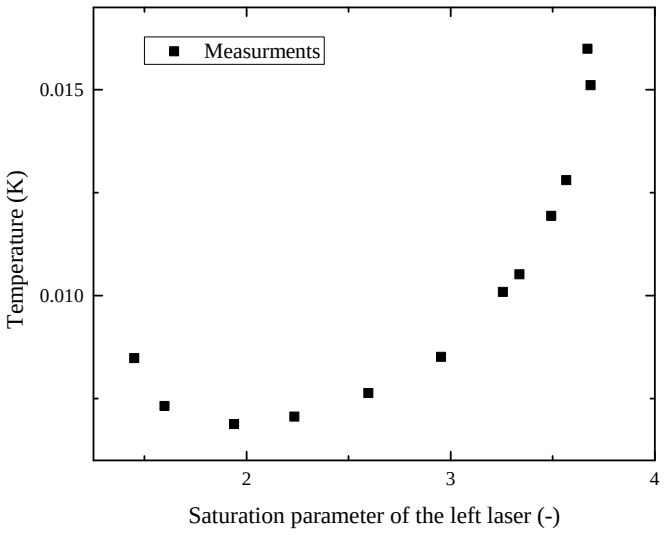

Figure 4.8: The temperature of the atomic beam against the saturation parameter of the left laser.

However, for the same angle, the temperature increases more with the imbalance than the magnetic field offset.

4.5 Conclusion

First the models, for both methods, are calculated to determine the average transverse velocity, which is proportional to the angle of the atomic beam with the z-axis if $\langle v_x \rangle \ll \langle v_z \rangle$. The formula for $\langle v_x \rangle$ with an magnetic field offset is equation (4.4). For the imbalance between the laser beam intensities the formula is equation (4.8). The simulations behaved as the analytical models, so this gives a first estimation that the analytical models make sense. After the simulations, experiments were done. The results showed that it was possible to steer an atomic beam with the two methods. The analytic model for the magnetic offset method is only verified in a qualitative way and the result of the imbalance gives an indication that the model somewhat correct, but not complete. It is not possible to shift the atomic beam without giving it an angle with the z-axis. This is because the cooling length is finite. The preferred model for steering is with the magnetic field offset. This is because it is linear and larger angles can be achieved.
The larger the angle of the atomic beam was, the higher the temperature became. The beam also became more asymmetrical. This was the inspiration to study the atomic beam profile of the cooled beam. This is done in the next chapter.

Chapter 5

The profile of the cooled atomic beam

The results of chapter 3 are as expected and there is no further research needed. In chapter 4, it is succeeded to steer the atomic beam in the cooling compression process with the help of an offset in the magnetic field or an imbalance in the laser beam intensities. However, these methods to steer the atomic beam had influence on the atomic beam profile, especially after some drift (in the third vessel). These effects are more that a shift of the profile and change in beam width (because of the cooling). This chapter is dedicated to explain the change in profile.

5.1 Deviation of the Gaussian profile

In the previous chapters, a Gaussian function with an offset is used to fit the atomic beam. However, the atomic beam profile does not have a perfect Gaussian profile. An example is given in 5.1. The peak position of the measurements and the fit have approximately the same position. The height of the peak is a bit off. The measured profiles have large tails compared to a Gaussian profile. They also have the same FWHM (full width at half maximum). This means that the average of the fit and standard deviation are approximately the same as the measurement. So the approximation This does not apply when the beam is steered in the cooling process. For example in figure 5.2. The fit and profile are only the same at some interception points, but the fit does not follow the profile smoothly. The peak positions do not align and because of the asymmetrical atomic beam profile, the standard deviation is not the same as the measurement.
These are two examples why the Gaussian function is not the best function to describe the atomic beam profile. Therefore an alternative distribution is researched in the next section. First the angular distribution is calculated.

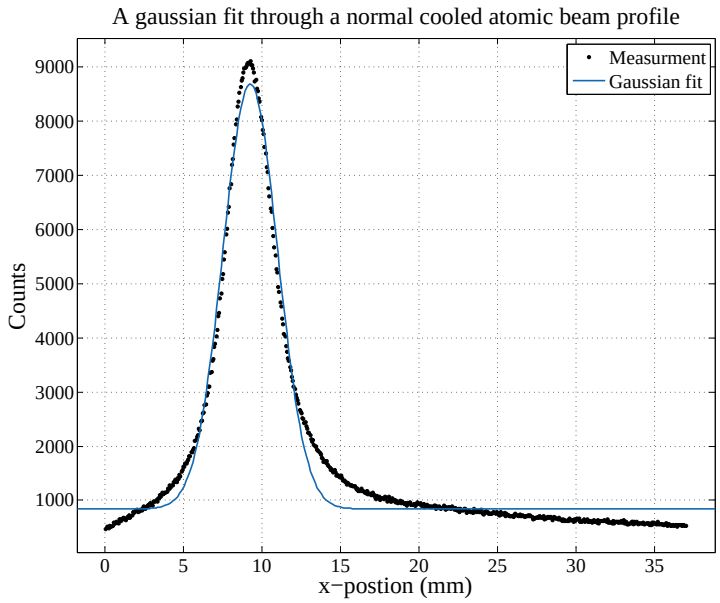

Figure 5.1: An example of a cooled atomic beam profile (third vessel) with a Gaussian fit. The laser intensities are in balance and there is no compression. The saturation parameter is for both laser beams $s_0 = 2.2$. The detuning of the laser beams is $\delta = -3.8$ MHz.

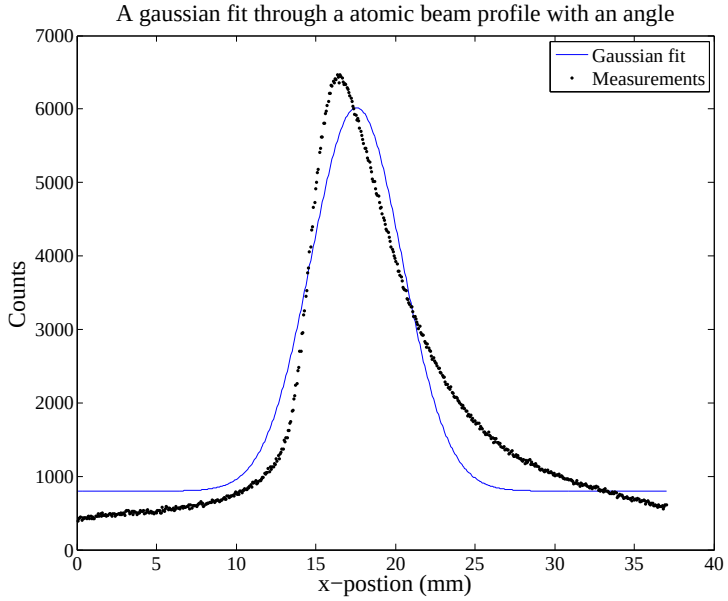

Figure 5.2: An example of a steered atomic beam profile (third vessel) with a Gaussian fit. The laser intensities are in balance and there is compression. The method of the offset in the magnet field is used as steering technique The saturation parameter is for both laser beams $s_0 = 2.3$. The current for the right coil is 0.08 A and for the other coils 0.01 A.

5.2 Angular distribution

The angular distribution $P_\theta(\theta)$ can be derived from the transverse and longitudinal velocity distributions. The longitudinal velocity distribution $P_{v_z}(v_z)$ is a Maxwell-Boltzmann distribution. This is because the source creates a Maxwell-Boltzmann distribution and the laser cooling has no influence on the longitudinal velocity. This means that the longitudinal velocity distribution is

$$P_{v_z}(v_z) = \sqrt{\frac{2}{\pi a^6}} v_z^2 \exp\left(-\frac{v_z^2}{2a^2}\right), \tag{5.1}$$

with $a = \sqrt{k_B T/m}$. The parameter a is for a rubidium-85 source at 100 °C around $a \approx 191$ m/s. This value determines also the average longitudinal velocity. This is $\langle v_z \rangle = a\sqrt{8/\pi} \approx 305$ m/s. The transverse velocity distribution P_{v_x} from the source can be approximated with a Gaussian distribution. This is if the assumption is made that the velocity is thermal distributed. When there is an imbalance in laser beam intensity or an offset in the magnetic field, the atomic beam gets an angle with z-axis. This means that $\langle v_x \rangle \equiv v_0 \neq 0$. This is compensated with an offset v_0 in the Gaussian distribution. So the transverse velocity distribution can be describe as

$$P_{v_x}(v_x) = \sqrt{\frac{1}{2\pi\sigma_{v_x}^2}} \exp\left(-\frac{(v_x - v_0)^2}{2\sigma_{v_x}^2}\right), \tag{5.2}$$

where v_0 is the offset created in the cooling process. To get the angular distribution, the variables v_x and v_z have to be rewritten to the angle θ with

$$\begin{cases} \theta &= \tan(v_x/v_z) \approx v_x/v_z \\ v_z' &= v_z \end{cases} \Longrightarrow \begin{cases} v_x &= \theta v_z' \\ v_z &= v_z' \end{cases} \tag{5.3}$$

In figure 5.3 is shown how theta is defined. Because $v_z \gg v_x$, the paraxial approximation is used.

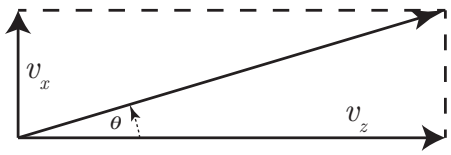

Figure 5.3: The longitudinal velocity is v_z and the transverse velocity is v_x. This means that $\theta = \tan(v_x/v_z)$

The transverse and longitudinal velocity are correlated. This is because the atoms with a low longitudinal velocity are cooled for a longer time. The assumption is made that the transverse and longitudinal velocity are correlated. This is because it will make the calculations easier. The assumption is possible because the two velocities are not heavily correlated, so the combined velocity distribution $P(v_x, v_z)$

is the product of equations (5.1) and (5.2). This is

$$P(v_x, v_z) = P_{v_x}(v_x) P_{v_z}(v_z). \tag{5.4}$$

To get the angular distribution $P_\theta(\theta)$, the change of variables formula[17] is used. This formula is for this case

$$P_\theta(\theta) = \int_0^\infty P(v_x, v_z)\, |\mathbf{J}|\, dv_z', \tag{5.5}$$

The matrix $\mathbf{J}$ is the Jacobian matrix of the inverse transformation in equation (5.3) and is defined as

$$\mathbf{J} = \begin{pmatrix} \frac{\partial v_x}{\partial \theta} & \frac{\partial v_x}{\partial v_z'} \\ \frac{\partial v_z}{\partial \theta} & \frac{\partial v_z}{\partial v_z'} \end{pmatrix} = \begin{pmatrix} v_z' & \theta \\ 0 & 1 \end{pmatrix}. \tag{5.6}$$

The determinant of $\mathbf{J}$ is $|\mathbf{J}| = v_z'$. With the transformation in equation (5.3), the velocity distribution in equation (5.4) and the determinant of equation (5.6), equation (5.5) will be

$$\begin{aligned} P_\theta(\theta) &= \int_0^\infty P(\theta v_z, v_z) v_z \, dv_z \\ &= \frac{1}{\pi a^3 \sigma_{v_x}} \int_0^\infty v_z^3 \exp\left(-\frac{v_z^2}{2a^2} - \frac{(\theta v_z - v_0)^2}{2\sigma_{v_x}^2} \right) dv_z, \end{aligned}$$

The solution of this integral is proportional to

$$P_\theta(\theta) \propto \left(v_0^2 \tilde{\theta}^2 \sigma_{v_x} + 2\tilde{\theta}^2 \sigma_{v_x}^3 + 2\sigma_{v_x}^5 \right) \zeta^{-6} + \sqrt{\frac{\pi}{2}} v_0 \tilde{\theta} e^{\chi^2} \left(3\sigma_{v_x}^4 + \tilde{\theta}^2 \left(v_0^2 + 3\sigma_{v_x}^2 \right) \right) (1 + \operatorname{erf}(\chi))\, \zeta^{-7} \tag{5.7}$$

where

$$\tilde{\theta} = a\theta,\ \zeta = \sqrt{\tilde{\theta}^2 + \sigma_{v_x}^2} \text{ and } \chi = \frac{v_0 \tilde{\theta}}{\sqrt{2}\sigma_{v_x} \zeta}.$$

In figure 5.4, the (not normalized) angular distribution is sketched for different v_0. For v_0, the distribution is symmetrical. The distribution gets less symmetrical if the atomic beam gets an average transverse velocity. This is because when the average transverse velocity increases the longitudinal velocity distribution dominates the angular distribution. This is probably also the reason why the temperature increases rapidly for bigger angles with the z-axis. The peak of the distribution changes also. The change in shape of the distribution is symmetrical for the average transverse velocity. This means that the distribution for $-v_0$ is the mirror image of the distribution for v_0 around the vertical axis. Equation (5.7) is a very complicated angular distribution, but if the atomic beam has no angle ($v_0 = 0$), equation (5.7) will reduce to

$$P_\theta(\theta) \propto \frac{1}{\left(a^2\theta^2 + \sigma_{v_x}^2\right)^2}, \tag{5.8}$$

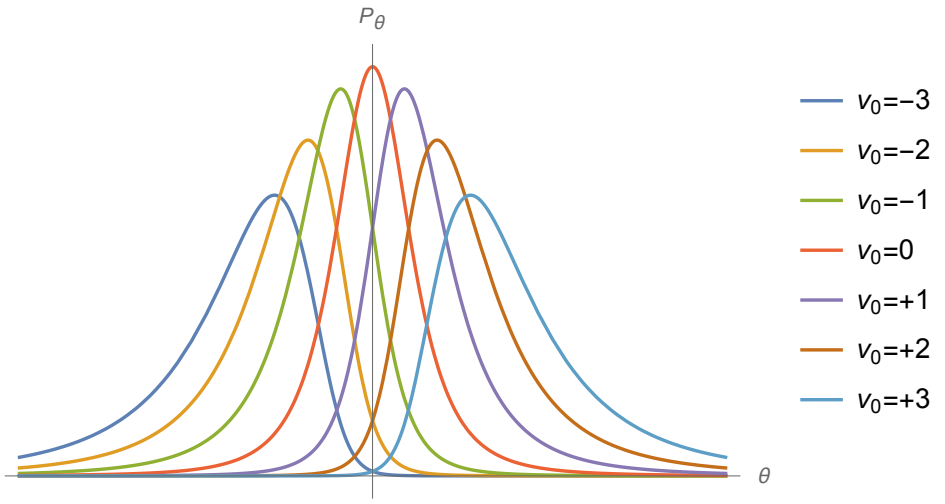

Figure 5.4: The angular distribution as function of the angle is sketched for different values of v_0, see the legend. The function is not normalized.

which is a squared Lorentz distribution. If the angular distribution can be measured and a is known, equation (5.7) can determine the average transverse velocity v_0 and the standard deviation of the transverse velocity σ_{v_x}. With σ_{v_x}, the temperature can be determined.
It is more difficult to find a position distribution. This is because it is difficult to determine where the atoms are coming from.

5.3 Comparison with the measured data

Like mentioned in the previous section, a position distribution is more difficult to calculate. This is because it is difficult to determine where the atoms are coming from. If the cooling and compression part is left out, the atomic beam can be traced back to a virtual beam source that can be approximated with a point source. Define the distance from the virtual point source to the measured profile as z_0 for the longitudinal direction and x_0 for the transverse direction (x_0 is not the offset created by the magnetic field here). The angle θ of an atom with the z-axis can now be determined with

$$\theta = \arctan \frac{\Delta x}{\Delta z} \approx \frac{x - x_0}{z_0}, \tag{5.9}$$

where x is the measured transverse position of the atom. The assumption is made that $\Delta x \ll \Delta z$. The measured beam profiles have an offset and are scaled, For a atomic beam with no angle, the profile can be described with equations (5.8) and (5.9) as

$$c = c_0 + \frac{A}{((x - x_0)^2 + b^2)^2}, \tag{5.10}$$

where c is the number of counts, c_0 the offset in the counts,A a scaling factor and $b = z_0\sigma_{v_z}/a$. The measured data in figure 5.1 is fitted with equation (5.10) in figure 5.5. The Squared Lorentz profile

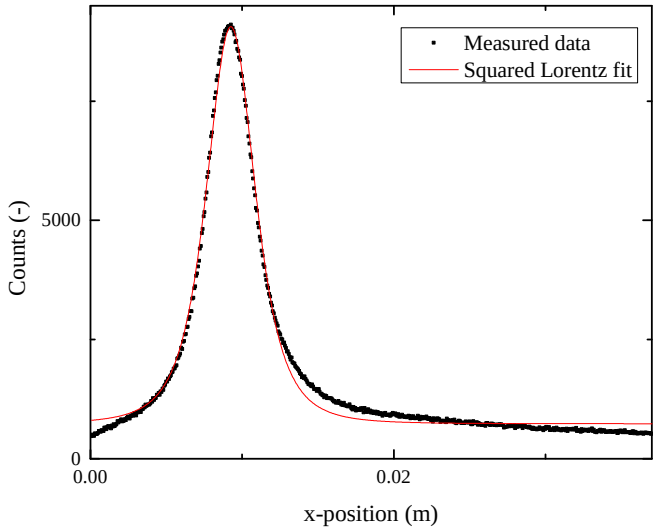

Figure 5.5: The measured atomic beam profile of figure 5.1 fitted with equation (5.10). The values of the fit parameters are $A = (6.3 \pm 0.1) \cdot 10^{-7}\,\mathrm{m}^2$, $c_0 = 734 \pm 8$, $x_0 = 0.00925 \pm 0.00001\,\mathrm{m}$ and $b = 0.00295 \pm 0.00002\,\mathrm{m}$.

describes the profile of an atomic beam with no angle better than the Gaussian profile. As the figures shows, equation (5.10) can describe the tails of the profile. The fit does not describe the right tail in this figure properly. This is probably because the laser beam intensities are slightly out of balance, so the beam has a very small angle.

The definition of b is known. So if a and z_0 are known, the value of σ_{v_x} can be determined and can be used to calculate the temperature. In principle, it is possible to measure the temperature now with just one profile instead of two. However, the value z_0 cannot be determined yet. It is possible to measure the temperature with two profiles. This will be discussed in the next section.

The previous fit is only valid if $v_0 = 0$. This is not the case if the atomic beam has an angle with the z-axis. Now the profile has to be described similar to equation (5.10), but with equation (5.7). This means that the profile in general can be described as

$$c = c_0 + Af(\frac{x - x_0}{z}), \tag{5.11}$$

where $f(\theta)$ is equation (5.7). Note that if $v_0 = 0$, this equation is reduced to equation (5.10). The parameters of this fit function are dependent on each other (excluding x_0 and c_0). To get preciser estimations of the parameters, two parameters are fixed. The values σ_{v_x} and v_0 are the parameters that are interesting, so a and z_0 are fixed. It is possible to get an estimation of a without this measurement.

This is $a \approx 191$ m/s. However, there is still no way to determine z_0. To check if equation (5.11) is a good description of the profile, a wild guess is made that $z_0 = 1$ m. The measured profile of figure 5.2 is fitted with equation (5.11) in figure 5.6. According this figure, equation (5.11) is a good description of

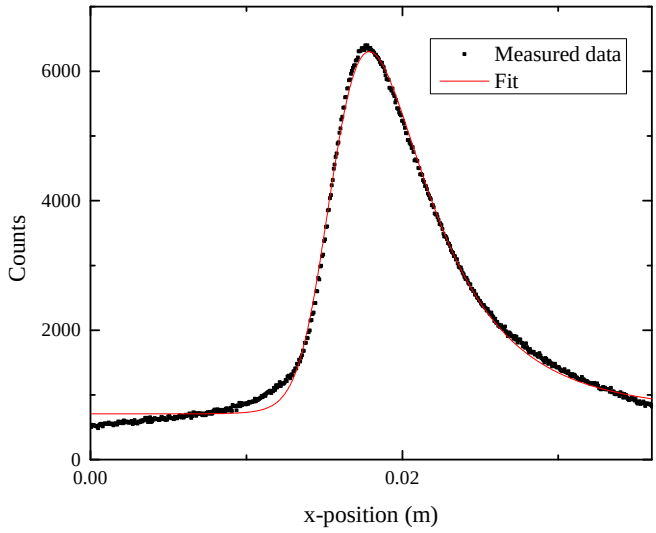

Figure 5.6: The measured atomic beam profile of figure5.2 fitted with equation (5.11). The values of the fit parameters are $c_0 = 705 \pm 6$, $A = (11 \pm 1) \cdot 10^2$ m^2, $a = 167$ m/s (fixed), $\sigma_{v_x} = 0.744 \pm 0.006$ m/s, $x_0 = 0.01238 \pm 7$ m, $v_0 = 1.90 \pm 0.02$ m/s and $z_0 = 1$ m (fixed).

the measured atomic beam profile if it has an angle, especially in comparison with the Gaussian fit. It describes the asymmetrical property and the long tails of the atomic beam. The fitted parameters are also accurate. The values of σ_{v_x} and v_0 look realistic. However, these values cannot be used to calculate the angle and temperature of the beam. This is because z_0 is not the proper value. For now, the value of z_0 is undetermined, but if there is a value of z_0 discovered in the future, this profile can describe the temperature and angle of the atomic beam.

5.4 Calculating the temperature with the squared Lorentz profile

Before the calculation of the temperature is discussed, the estimation of the fit parameters of equation (5.10) will be treated. The parameters c_0 and x_0 are the easiest to estimate. The estimation of c_0 is just the minimum value of counts and the value of x_0 is just the x-position value of the profile's peak. The value of b can be estimated with the FWHM (Full width at half maximum) and this can be guessed

from the profile shape. The FWHM of a function $f(x)$ is defined as

$$\text{FWHM} = x_2 - x_1, \text{where } x_1 \text{ and } x_2 \text{ are the solutions of } x \text{ for } f(x) = \frac{1}{2} f(x_{max}),$$

where x_{max} is the x-position of the maximum. The values for x_1 and x_2 are for equation (5.10) (without offset c_0)

$$x_1 = x_0 - b\sqrt{\sqrt{2} - 1} \wedge x_1 = x_0 + b\sqrt{\sqrt{2} - 1}$$

So the value for the FWHM is

$$\text{FWHM} = 2b\sqrt{\sqrt{2} - 1} \approx 1.28719 \cdot b,$$

so b can be estimated with $b = \text{FWHM}/1.28719$. The last parameter to be estimated is A. This can be done with the height of the peak. The peak of a squared Lorentz is always at x_0. The height of the peak is then $c_{max} = c_0 + A/b^4$. The parameters c_0 and b are already estimated, so the estimation of A is $A = b^4(c_{max} - c_0)$. With these estimations, equation (5.10) can be faster fitted to measured data.
A method to calculate the temperature is discussed in subsection 2.3.2. The formula was equation (2.8). This method used the standard deviation of two measured atomic beam profiles approximated with a Gaussian. Like discussed in the previous section, a squared Lorentz is a better description of the atomic beam profile. Unlike the normal Lorentz distribution, the standard deviation can be calculated easily for a squared Lorentz. The normalized squared Lorentz is

$$P(x) = \frac{2b^3}{\pi((x - x_0)^2 + b^2)^2}.$$

The variance σ_x^2 is then

$$\begin{aligned}
\sigma_x^2 &= \langle x^2 \rangle - \langle x \rangle^2 \\
&= \int_{-\infty}^{\infty} x^2 P(x)\, dx - \left(\int_{-\infty}^{\infty} x P(x)\, dx \right)^2 \\
&= b^2 - x_0^2.
\end{aligned}$$

So instead of fitting a Gaussian, it is more accurate to fit a squared Lorentz and take the standard deviation of this and use with equation (2.8).
Another method to calculate the temperature is with the parameter σ_{v_x} in equation (5.8). The problem was that z_0 cannot yet be determined. However, this problem can be bypassed with two measured atomic beam profiles. First, measure the two atomic beam profiles (the first after the cooling and the second after drift in the third vessel). Both profiles can be fitted with equation (5.10). Note that the parameter $b = z_0\sigma_{v_z}/a$. Because there is no cooling between the two measured profiles the values of σ_{v_z} and a are constant, only z_0 changes. There is a relation between the two z_0. Lets say that in the second

profile $z_{0,2} = z_0$. This means that $z_{0,2} = z_0 - \Delta z$, where $\Delta z = 580\,\text{mm}$ is the distance between the cameras.This means that parameter b directly after cooling is $b_1 = \frac{\sigma_{v_x}}{a}(z_0 - \Delta z)$ and after drift (third vessel) $b_2 = \frac{\sigma_{v_x}}{a} z_0$. The values of b_1 and b_2 can be determined with a squared Lorentz. This means that

$$\begin{cases} b_1 &= \frac{\sigma_{v_x}}{a}(z_0 - \Delta z) \\ b_2 &= \frac{\sigma_{v_x}}{a} z_0 \end{cases} \Rightarrow \begin{cases} \sigma_{v_z} &= \frac{a}{\Delta z}(b_2 - b_1) \\ z_0 &= \frac{b_2 \Delta z}{b_2 - b_1} \end{cases} \tag{5.12}$$

The standard deviation of the transverse velocity can now be determined without knowing z_0. Even z_0 can be calculated. However, z_0 is not constant value for different circumstances. This distance is dependent on the cooling and compression process probably.
In figure 5.7 the measured atomic profile right after cooling is shown. This is from the same measurement as figure 5.5 (this in in the third vessel). This is an other example why the Squared Lorentz is a

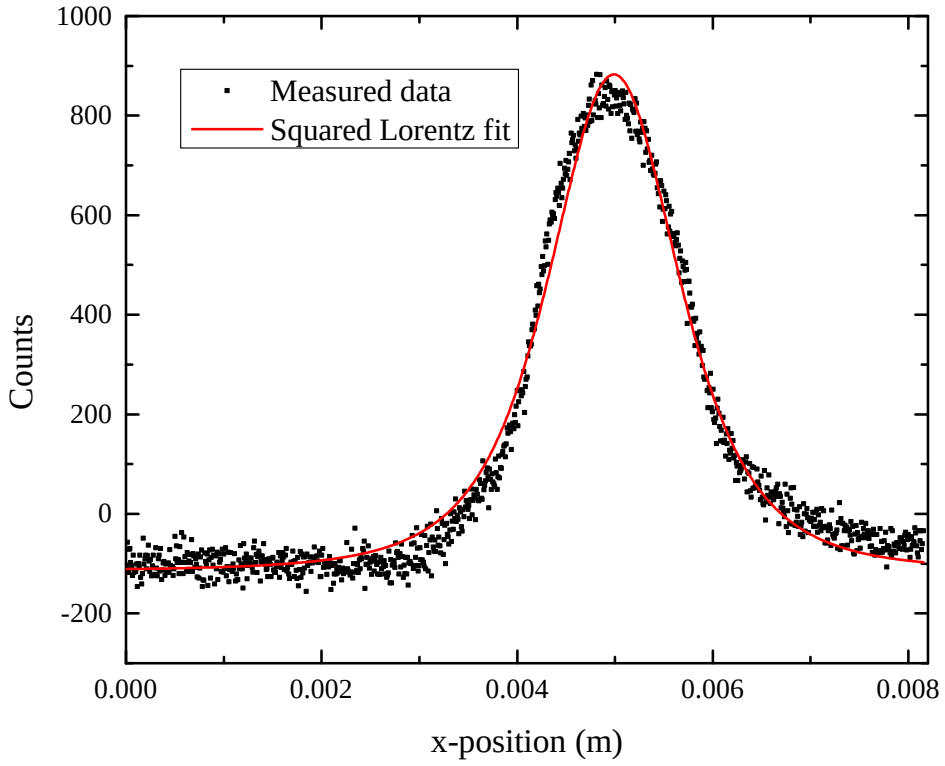

Figure 5.7: The measured atomic beam profile in the first vessel. This is from the same measurement as figure 5.5 (third vessel). Equation (5.10) is used to fit the data. The fit parameters are $A = (2.24 \pm 0.06) \cdot 10^{-9}\,\text{m}^2$, $c_0 = -114 \pm 2$ and $b_1 = 0.00122 \pm 0.00001\,\text{m}$.

good description of the profile (if the beam has no angle with the z-axis). From the result of figures 5.5 and 5.7 follows that $b_1 = 0.00122\,\text{m}$ and $b_2 = 0.00295\,\text{m}$. With $\Delta z = 0.58\,\text{m}$ and $a = 168\,\text{m/s}$, the

values of σ_{v_x} and z_0 can be determined. These values are $\sigma_{v_x} = 0.5\,\text{m/s}$ and $z_0 = 1\,\text{m}$. This means that the temperature measured with the help of equation (5.12) of the atomic beam is $T = 5\,\text{mK}$. When the temperature for this atomic beam is measured with Gaussians and equation (2.8), it is $T = 7\,\text{mK}$. This means that the temperature calculated with the new method has a realistic value. It is a bit lower than the old method. The method with equation (5.12) is probably more accurate. This is because the longitudinal velocity distribution is included. A similar method is not found for the situation when the atomic beam has an angle. This is because equation (5.11) is to complicated.

5.5 Conclusion

The measured atomic beam profile is in the previous chapters approximated with a Gaussian profile. It does not describe the atomic beam profile completely. If the beam has no angle with z-axis, it gives a good indication of the standard deviation of the beam and the position. It does not explain the relative long tails of the atomic beam profile. This is not characteristic for a Gaussian. When the atomic beam has an angle with the z-axis, the Gaussian does not fit the profile anymore. A different function is found to describe the profile. This function is reduced to a squared Lorentz if the the atomic beam has no angle. This function also explained why the temperature increase significant when the atomic beam is steered. This is because then the longitudinal velocity dominates the angular distribution, which is related to the position distribution. The new profile for atomic beams without angles brings also an alternative method to calculate the temperature of the beam with it. This method gives realistic values and is probably more accurate because the longitudinal distribution is included.

Chapter 6

Conclusion

The overlapping subject of this report was laser cooling and compression of atomic rubidium for the ABLIS project. First the theory was discussed and the setup of the simulations and experiments for this project. The first research was about the effect of the aberrations of the cooling laser to the cooling of the atomic beam. These aberrations are caused by the cylindrical telescope that is used to expand the laser. The optimal lens distance is defined as the distance between the two lenses of the telescope which achieve the lowest atomic beam temperature. The optimal lens distance was predicted at 11.36 cm. According the simulations that were done the optimal lens distance is between 11.3 cm and 11.5 cm, which agrees with the predicted value. The optimal lens distance found with the experiments is between 10.8 cm and 11.3 cm. This is just under the predicted value. However, the temperature did not change extremely around these ranges. This means that the lens distance is not precision work, it has no significant influence on the cooling if the lenses are 1 mm off the optimal lens distance. The conclusion is that the aberrations have minimal influence on the laser cooling for a certain range. No further research is needed for this topic.

The main topic of this report is about the possibility to steer the atomic beam in the cooling process. Two methods are discussed. The first method was with creating an offset in the magnetic field. A linear relation was found between the average transverse velocity of the atomic beam and the offset of the magnetic field. It was not possible to shift the atomic beam without giving the beam an angle with the longitudinal axis. This is because the cooling length is finite. Shifting the atomic beam without giving the beam an angle with the longitudinal axis is possible if the cooling length is $L_c \gg 0.0\,\mathrm{m}$. The simulations agreed with the analytical model. For the experimental results, only a qualitative comparison is done with the analytical model. The relation between the offset and the average transverse velocity is linear, as expected. The temperature rises when the beam gets an angle.

The other method to steer the atomic beam is with an imbalance in laser beam intensities. The analytical model predicts that the average transverse velocity is not a linear function of the intensity of the laser beams. The results, for angle versus the imbalance, of the analytical model are according the analytical model quantitative and qualitative. Steering of the beam is also observed in the experiments.

The results had the same shape as the model, but not quantitatively. This is because the assumption is made that the transverse velocity of every atom in the beam is zero, because $\langle v_x \rangle = 0$. This is however not the case for the experiments. Again the temperature increased significantly when the beam was steered.
The preferred steering technique is with the magnetic field. This is because the relation between the magnetic field offset and the average transverse velocity is linear, and the temperature increases less for the same angle of the beam in comparison to the imbalance of laser beam intensity.
When the atomic beam has an angle, the shape of the angular distribution of the atomic beam changes. An alternative function is found to describe the beam profile. This function can explain the asymmetrical property of the beam when it gets an angle with the z-axis. This is because when the beam gets an angle, the longitudinal velocity distribution dominates the angular distribution that is related to the atomic beam profile. The new profile for atomic beams without angles brings also an alternative method to calculate the temperature of the beam with it. This method gives realistic values and is probably more accurate because the longitudinal distribution is included.

6.1 Outlook

As mentioned before the effects of the aberrations does not require further research. For the steering part, a quantitative check for the analytical model can be done. To get more control over the beam, a combination of the two methods is maybe worth looking in to. Maybe it is possible to steer the beam with one method and with the other try to correct the asymmetrical property of the spatial profile of the beam. Maybe then it is possible to steer the atomic beam without a significantly increase of temperature.
Further research in the atomic beam profile is needed. If it is possible to determine the position of the virtual point source, the temperature of the beam and the angle can be determined with just one camera.

Bibliography

[1] S. Reyntjens and R. Puers, J. Micromech. Microeng. **11**, 287 (2001).

[2] G. ten Haaf, Atomic beam laser-cooled ion source: towards sub-nm ion beam milling, Master's thesis, Technische Universiteit Eindhoven, 2013.

[3] G. ten Haaf, S. Wouters, S. van der Geer, E. Vredenbregt, and P. Mutsaers, J. Appl. Phys. **116**, 244301 (2014).

[4] M. P. Reijnders, *Ion beams from laser-cooled gases*, PhD thesis, Technische Universiteit Eindhoven, 2010.

[5] S. Chu, Rev. Mod. Phys. **70**, 685 (1998).

[6] C. N. Cohen-Tannoudji, Rev. Mod. Phys. **70**, 707 (1998).

[7] W. D. Phillips, Rev. Mod. Phys. **70**, 721 (1998).

[8] C. J. Foot, *Atomic physics*, OUP Oxford, 2004.

[9] E. Vredenbregt and K. Van Leeuwen, Am J Phys **71**, 760 (2003).

[10] B. Jansen, Atomic beam source for the ultracold focused ion beam setup, Master's thesis, Technische Universiteit Eindhoven, 2013.

[11] J. van Rens, Laser cooling of a rubidium beam, Master's thesis, Technische Universiteit Eindhoven, 2014.

[12] G. van Pamelen, Charactersation of an in-vacuum magnetic quadrupole for a 2d magneto-optical compressor, Bachelor's thesis, Technische Universiteit Eindhoven, 2015.

[13] D. A. Steck, Rubidium 85 d line data, 2013, available online at http://steck.us/alkalidata.

[14] Thorlabs, Lj1895l1-b, 2010, available online at http://www.thorlabs.de/thorproduct.cfm?partnumber=LJ1895L1-B.

[15] Thorlabs, Lk1753l1-b, 2010, available online at http://www.thorlabs.de/thorproduct.cfm?partnumber=LK1753L1-B.

[16] S. H. W. Wouters et al., Phys. Rev. A **90**, 063817 (2014).

[17] K. Lange, *Applied Probability*, Springer New York, 2010.

Appendix A

Coefficients of the angular distribution

This appendix contains the calculations of the coefficients from table 3.1. The angular distribution for different lens distances is measured wit a ray tracer. These are fitted with equation (3.1). An example of a angular distribution is given in figure 3.1. The functions of the coefficients are plotted in figure A.1

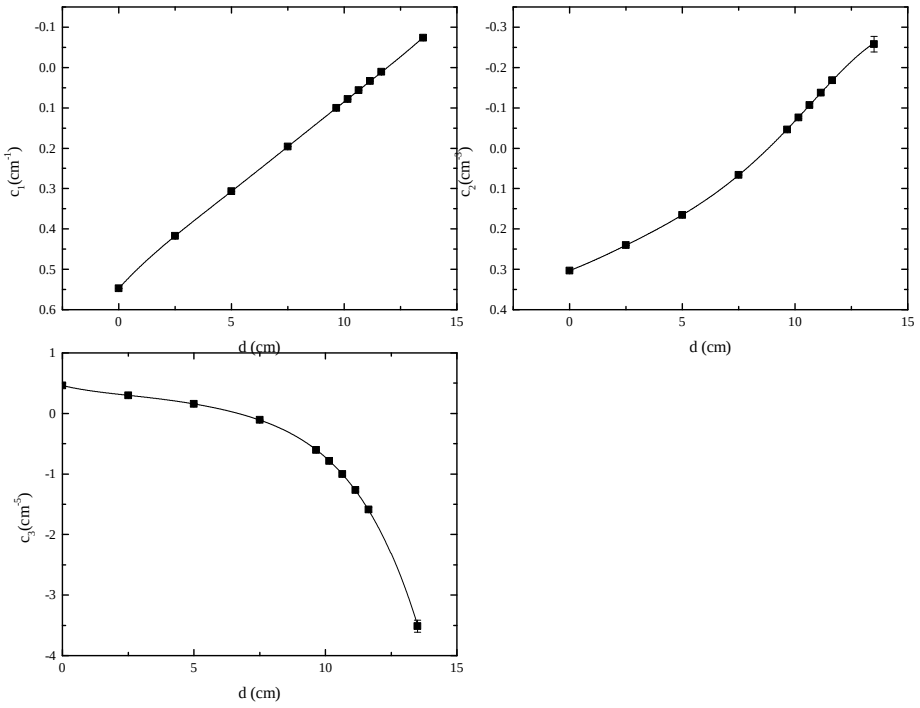

Figure A.1: Top left is the function for the first coefficients as function of the lens distance. Top right is the function for the second coefficients as function of the lens distance. Bottom left is the function for the third coefficients as function of the lens distance.